A continental reconstruction of hydroclimatic variability in South America during the past 2000 years

Mathurin A. Choblet[1,2,3], Janica C. Bühler[3], Valdir F. Novello[3], Nathan J. Steiger[4,5], and Kira Rehfeld[3]

[1]Department of Astrophysics, Geophysics and Oceanography, University of Liège, Liège, Belgium
[2]Institute of Environmental Physics, Heidelberg University, Heidelberg, Germany
[3]Department of Geosciences, University of Tübingen, Tübingen, Germany
[4]Hebrew University of Jerusalem, Jerusalem, Israel
[5]Lamont-Doherty Earth Observatory, Columbia University, Palisades, NY, USA

Correspondence: Mathurin A. Choblet (mathurin@choblet.com)

Abstract. Paleoclimatological field reconstructions are valuable for understanding hydroclimatic variability. While being similarly impactful on societies as temperature variability, hydroclimatic variability has still remained less in focus. However, reconstructing globally complete fields of climate variables lacks adequate proxy data from tropical regions like South America, limiting our understanding of past hydroclimatic changes in these areas. This study addresses this gap using low resolution climate archives, including speleothems, previously omitted from reconstructions. Speleothems record climate variations on decadal to centennial time scales and provide a rich dataset for the otherwise proxy data scarce region of tropical South America. By employing a multi-time scale Paleoclimate Data Assimilation approach, we synthesize climate proxy records and climate model simulations, capable of simulating water isotopologues in the atmosphere, to reconstruct 2000 years of South American climate. This includes surface air temperature, precipitation amount, drought index, isotopic composition of precipitation amount, and the intensity of the South American Summer Monsoon. The reconstruction reveals anomalous climate periods: a wetter and colder phase during the Little Ice Age (∼1500 - 1850 CE) and a drier, warmer period corresponding to the early Medieval Climate Anomaly (∼600 - 900 CE). However, these patterns are not uniform across the continent, with climate trends in northeastern Brazil and the Southern Cone not following the patterns of the rest of the continent, indicating regional variability. The anomalies are more pronounced than in previous reconstructions, but match trends found in local proxy record studies, thus highlighting the importance of including speleothem proxies. The multi-timescale approach is essential for reconstructing multi-decadal and centennial climate variability. Despite methodological uncertainties regarding climate model biases and proxy record interpretations, this study marks a crucial first step in incorporating low resolution proxy records as speleothems into climate field reconstructions using a multi-timescale approach. Adequately extracting and using the information from speleothems potentially enhances insights into past hydroclimatic variability and hydroclimate projections.

1 Introduction

The climate of the Common Era (CE), which spans the last two millennia, is considered the most thoroughly studied prein-dustrial paleoclimatic period owing to the abundance of records from various paleoclimate archives (PAGES 2k Consortium, 2019) and climate observations. It provides rather stable, close to present-day boundary conditions prior to the onset of in-

25 dustrialization with relatively constant greenhouse gas concentration and sea level, and climate variability due to natural, solar and volcanic forcings. Thus, it represents a well-studied benchmark for climate models (e.g. Jungclaus et al., 2017). Over the last two millennia, the global climate presents itself as an interplay and superposition of various major atmospheric and oceanic modes of variability. As such, different regions of South America are influenced by the El Niño-Southern Oscillation (ENSO), the Pacific Decadal Oscillation (PDO), the Atlantic Multidecadal Oscillation (AMO), the Southern Annular Mode

30 (SAM) and variations in the position of the Intertropical Convergence Zone (ITCZ) (Garreaud et al., 2009). The spatial and temporal variability of the South American Summer Monsoon (SASM) (Zhou and Lau, 1998; Marengo et al., 2010) and its sub-component, the South Atlantic Convergence Zone (SACZ) (Carvalho et al., 2004), create a wide range of climate zones across the continent. This makes the South American continent an intriguing testbed for climatological research of the interplay of different phenomena before the onset of the current warming period.

35 The challenges posed by anthropogenic climate change are particularly pronounced in South America. The implications for water resources are significant, given that South America comprises two of the world's most crucial river basins: the Amazon Basin in the center-north and the Parana/La Plata Basin in the center-southeast. However, the broader effects of anthropogenic climate change on the entire hydrological cycle and its variability, including changes in precipitation extremes and the occurrence of droughts, remain less studied than for temperature. Improving the understanding of the full range of

40 climate variability in South America is imperative, given the high vulnerability of human livelihoods in tropical and subtropical regions to the impacts of climate change. This vulnerability is especially evident in extreme events like droughts and floods, due to both geographic and socioeconomic factors (Pörtner et al., 2022), as seen for example in the current megadrought in central Chile (Garreaud et al., 2019).

The climate of the past beyond the instrumental period is studied to enhance our understanding of hydroclimate and contex-

45 tualize recent changes. For instance, extreme events and their socioeconomic consequences have been recorded in historical documents (Prieto and García Herrera, 2009), such as a sequence of drought in northeastern Brazil (Aceituno et al., 2008; Utida et al., 2023), droughts in Bolivia (Gioda and Prieto, 1999), and extreme floodings of the Parana River (Prieto, 2007).

Climate archives are increasingly used to reconstruct and interpret changes in climate beyond the instrumental era. These reconstructions offer statistically robust estimates of the climate, particularly for the CE, the period of interest in our study. In

50 principle, existing global climate field reconstructions of the CE already provide estimates for both surface temperature and hydroclimate variables, including for South America (e.g., Hakim et al., 2016; Franke et al., 2017; Steiger et al., 2018; Tardif et al., 2019; Neukom et al., 2019). However, global CE reconstructions predominantly rely on proxy records from the mid-to-high latitudes, particularly tree rings from the Northern Hemisphere. Climate proxy record density for the CE in tropical and subtropical regions is much lower, in particular for terrestrial locations (Neukom and Gergis, 2012). Terrestrial proxy

records are, however, crucial, when it comes to reconstructing hydroclimatic variability. Although climate field reconstruction can make use of teleconnections to alleviate data scarcity, the lack of local data limits the viability of global reconstruction in (sub-)tropical regions (Anchukaitis and Smerdon, 2022).

For South America, climate field reconstructions are constrained by the scarcity of climate proxy records for all regions except for the central and southern Andes, where tree rings serve as an abundant climate archive. Regional climate field reconstructions have thus primarily focused on Southern South America (Neukom et al., 2010, 2011; Boucher et al., 2011; Luterbacher et al., 2011; Morales et al., 2020). However, in recent years speleothems have emerged as a promising climate archive with the potential to alleviate data scarcity in tropical South America (Vuille et al., 2012). Speleothems are geological cave formations created by accumulating layers of calcium carbonates transported by seepage water. Among the many climate proxies archived in speleothems, the ratio between heavy and light oxygen isotopes (δ^{18}O) as saved in accumulating layers of calcium carbonate reflects the isotopic composition of the precipitation above a cave and, thus, records hydroclimatic changes (Bradley, 2015). The δ^{18}O signatures of precipitation are sensitive to air temperature, precipitation amount changes, and the geographical location in terms of altitude, latitude, and distance from the coast (Dansgaard, 1964). For South America, in particular the SASM influenced region, the rainfall amount during the monsoon season is a primary driver on the $\delta^{18}O$ signatures of precipitation (Vuille et al., 2003; Moquet et al., 2016)

Tropical South America is an archetypical region for speleothem research with a growing number of published records in recent years. For instance, single records have been used to demonstrate changes in the intensity of the SASM on millennial to centennial time scales in response to changes in orbital and solar forcing (Novello et al., 2016; Bernal et al., 2016). For the hydroclimate of the last millennium, pronounced anomalies found in speleothem δ^{18}O values have been associated to the Medieval Climate Anomaly (MCA) and the Little Ice Age (LIA) (Novello et al., 2018; Apaéstegui et al., 2018; Azevedo et al., 2019). Moreover, through the analysis of several South American speleothem records using dimensionality-reduction techniques, Orrison et al. (2022) demonstrated that climate model simulations of the last millennium consistently underestimate centennial climate changes over the South American continent, reinforcing findings of Rojas et al. (2016), who investigated SASM variability in climate model simulations.

It is not clear, if existing climate field reconstructions include these insights into South American Hydroclimate variability during the CE due to the limited integration of speleothem records. Their incorporation proves difficult for two main reasons. First, reconstructions of the CE are usually attempted at seasonal or annual resolution and, thus, only include proxy records of at least annual resolution. Speleothems are seldom dated annually with dating uncertainties often on the scale of several years. Even so, karst processes above the caves work as smoothing filters of the isotopic variations in precipitation. Thus, speleothem δ^{18}O time series reflect the mixing of rainfall from different seasons and the transit time through the epikarst to the water dripping point in the cave (for speleothems in Brazil see Moquet et al., 2016). Second, climate field reconstructions usually require a calibration of the proxy records against instrumental data. This calibration is hampered by the low temporal resolution of speleothem records and short data overlap with regional instrumental observations. Similar restrictions also apply to many lake and marine sediments, precluding their use in current climate field reconstructions. In this study, we aim to overcome

these limitations to explore the information gain associated with including previously excluded climate archives of annual to decadal resolution.

Here, we present the first climate field reconstruction of the hydroclimate of the South American continent for the entire CE, employing speleothems besides more commonly-used climate archives such as tree rings, lake sediments, ice cores, corals, sclerosponges, marine sediments and historical documents. We combine proxy records from a multitude of proxy record databases (Emile-Geay et al., 2017; Comas-Bru et al., 2020; Konecky et al., 2020; Morales et al., 2020; Neukom et al., 2009) and individual records provided by original authors. This yields a total of 307 proxy records (See Figure 1). Our selection represents the at present spatially most complete collection of publicly available proxy record data for the region.

As a climate field reconstruction technique, we choose Paleoclimate Data Assimilation (PaleoDA) (Bhend et al., 2012; Steiger et al., 2014). Based on the principles of DA, which has been successfully applied in weather and ocean forecasting for three decades (Evensen et al., 2022), PaleoDA fuses information from climate model simulations and climate observations to provide a best state estimate. In contrast to other regression-based techniques (e.g Principal Component Regression as in Luterbacher et al., 2002; Neukom et al., 2014), PaleoDA does not directly rely on gridded instrumental datasets. The climate simulations provide time series long enough to also include proxy records of relatively low resolution, such as speleothems, which cannot be calibrated to instrumental data. We use five state-of-the-art isotope-enabled climate simulations, which simulate the isotopic composition of precipitation and which were made publicly available recently (Bühler et al., 2022). Employing these previously unused simulations in PaleoDA provides a twofold information gain: first, it enables the inclusion of speleothem records in the PaleoDA without the uncertainties associated with instrumental calibration, and second, it facilitates the comparison of multiple simulations of rainfall δ^{18}O values from different models, thereby mitigating biases stemming from individual proxies and models. In this study, we will focus on surface temperature, precipitation amount, the drought index SPEI (Standardized Precipitation Evapotranspiration Index, Vicente-Serrano et al. (2010); Beguería et al. (2014)), and the isotopic composition of precipitation. While in theory, PaleoDA allows reconstructing climate fields for all simulated climate variables, the chosen variables are most closely related to the climate signal recorded by the selected climate archives and, thus, hold the highest potential for reliable reconstructions. To overcome the difficulties posed by proxy records of annual to decadal resolution such as speleothems, we adapt the PaleoDA algorithm to a multi-timescale method enhancing the concept proposed by Steiger and Hakim (2016).

The structure of this study is as follows: We introduce the proxy record and climate model simulation data on which we base our reconstruction. We then provide a complete description of the multi-timescale PaleoDA methodology, its assumptions and key parameters. We present our obtained reconstruction (for both annual and austral summer means) and validate it by means of comparison to instrumental data, other reconstructions, and non-assimilated proxy record data. As one of several climatological applications of the reconstruction dataset, we study the main centennial hydroclimatological changes in South America during the MCA and the LIA and assess if our reconstruction aligns with insights from other studies. In addition, we investigate the reconstructed intensity and variability of the SASM using a precipitation-based monsoon index, which has not been studied in climate field reconstructions before.

2 Data

2.1 Paleoclimate Proxy Data
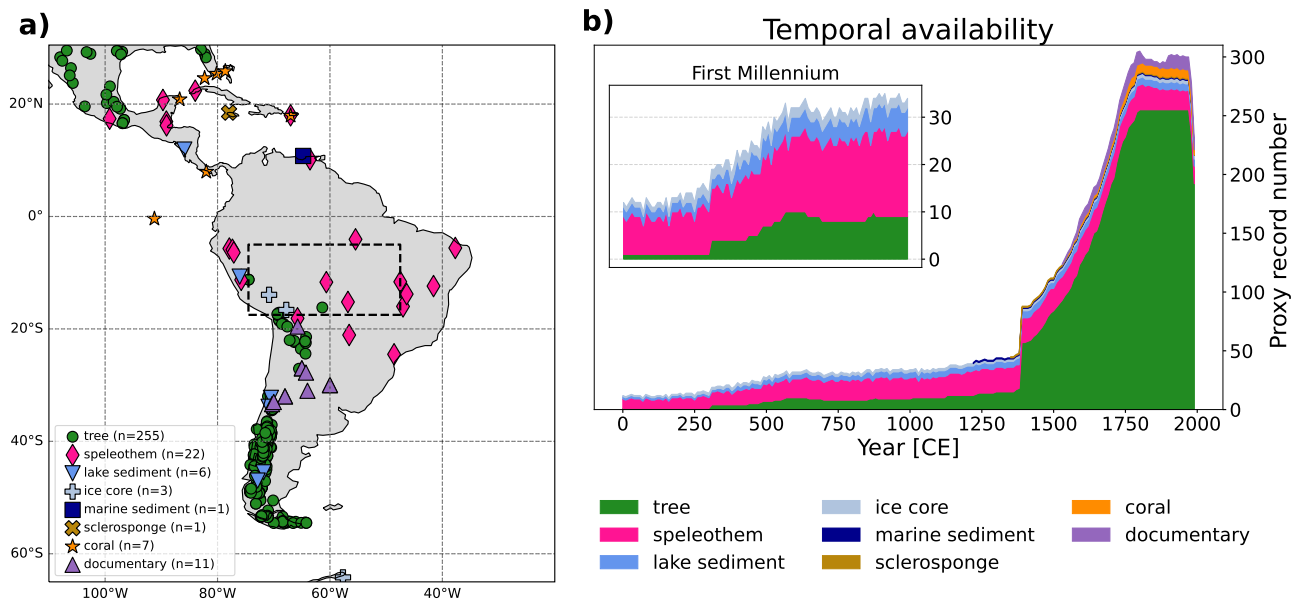
Figure 1. Spatiotemporal availability of the employed proxy records. a) Spatial distribution of all employed proxy records. Archive types are encoded by shape and color. The represented spatial domain (65°S-35°N, 20°W-110°W) is the spatial domain reconstructed in this study. In addition, the black box demarcates the core region of the South American Summer Monsoon (SASM) following the definition by Vuille et al. (2012), which we use to reconstruct the SASM index. b) Temporal availability of proxy archive types, with a zoom on the first millennium.

125   The continental climate field reconstruction provided in this study is based on a selection of different climate archive types. While focusing on climate archives that store information about the hydroclimate, we also include other types of archives for better covering the range of variables. The archives include trees, speleothems, ice cores, lake sediments, corals, sclerosponges and marine sediments. To ensure the best possible spatio-temporal coverage of the region, we have chosen and combined proxy records from three published paleoclimate proxy databases: PAGES2k (Emile-Geay et al., 2017) , Iso2k (Konecky et al., 2020),

130   the third version of the database from then Speleothem Isotopes Synthesis and AnaLysis group SISALv3 (Atsawawaranunt et al., 2018; Comas-Bru et al., 2020; Kaushal et al., 2023), tree rings used for the South American Drought Atlas (Morales et al., 2020) and historical documentary indices presented by Neukom et al. (2009). We additionally included single proxy records which are currently not part of published proxy record databases (individual references in Appendix A1). In contrast to the other proxy record databases, the SISALv3 speleothem database has not been employed in climate field reconstruction

135   previously.

The SISALv3 database provides different sets of chronologies for the different speleothems. For this analysis, we use the authors' original chronology only. Further, age uncertainties, which are only provided for SISALv3, are not explicitly considered as these are mostly smaller than the timesteps in the multi-time scale PaleoDA algorithm (see Section 3.2). A description table for each climate archive type that we included, including metadata for the individual proxy records, the proxy variable, median resolution and methodological choices (Proxy System Model, assumed noise, seasonality, time scale) is provided in the Appendix Tables A1 to A7.

We define four selection criteria for choosing proxy records from the respective databases:

1. The sites where the climate archives where obtained are located in the region 65°S-35°N, 20°W-110°W (See Figure 1). Proxy records from Central America are explicitly included as they can provide information for the northern part of South America, where few proxy records for the past two millennia exist.

2. The proxy variable is approximately linearly related to one of the climate variables provided by the climate model simulations (see Section 2.2 and 3.3). We follow the recommendations given by the authors in the original publications to decide if such a relationship holds. Note, that speleothem and ice core $\delta^{18}O$ values can also be included in our proxy record collection because the climate model data also includes simulated isotopic-composition of rainfall.

3. The proxy records span at least 200 years and have at least one sample value in the period from 1750 to 1850 CE. This period is used as the reference period for computing anomalies of the proxy records relative to a shared time period. It has the advantage of including crucial records as speleothems, that lack data points during the more commonly chosen reference period of the 20th century. At the same time, this excludes many shorter records which would lead to high reconstruction skill during the instrumental era, but would not contribute to the reconstruction of centennial scale hydroclimate changes, and are, thus, acceptable to omit.

4. The resolution of the proxy records is better than 10 years (median), as we set 10 years as the largest reconstruction time scale in the multi-time scale PaleoData Assimilation approach (described in the Section 3.2). While decadal to multi-decadal and lower resolution is technically possible, the proxy records falling into that category are too coarsely resolved to contribute to the skill of the reconstruction of the past two millennia on multi decadal and centennial time scales, which is the focus of this study.

Our selection of proxy records for the South American reconstruction consists of 307 records covering southern and central America (Figure 1). Due to our selection criteria, the maximum number of proxy records is available in the reference period 1750 - 1850 CE and the least in the first century (13 records). Despite the decreasing number of available proxy records back in time during the CE, the spatial coverage remains fairly similar throughout time, as older proxy records are evenly distributed. This is particularly evident for tree rings, which are clustered in the Andes (see also AF A1 for the spatiotemporal availability of proxy records for each reconstructed century). The temporal availability of proxy records shows a sharp decline in tree ring data in the year 1400 CE, coinciding with the start of the SADA tree ring database. Throughout the reconstruction, we remain attentive to potential artifacts resulting from this decline. Despite this concern, we anticipate only a small impact, given that

the tree rings are situated in regions where there are already existing proxy records. Non-speleothem archives mostly cover the central and southern Andes and coastal regions, while speleothems significantly contribute to the coverage of tropical inner-continental regions over the entire two millennia. Regions lacking archive sites for proxy records can be found in the northern part of South America, namely Colombia, the Guianas and the north western states of Brazil. Additionally, the western part of the Southern Cone, the cone-shaped area of South America south of the Tropic of Capricorn ($\sim$23.4°S), lacks proxy records. However, the South American Drought Atlas has demonstrated that tree ring records from the central and southern Andes can be skillfully used to reconstruct the hydroclimate of that region. The northern part of the Southern Cone is covered by documentary data from the 16th century on.

2.2 Isotope-enabled climate model simulations

We use five state-of-the-art isotope-enabled climate model simulations of the last millennium (Bühler et al. (2022) and Table 1). Additional information about boundary conditions and forcing parameters can be found in Bühler et al. (2022). Isotope-enabled climate models are essential for our study as they allow us to bypass the uncertain calibration of speleothem δ^{18}O records to temperature or precipitation. The isotopic composition of precipitation (δ^{18}O values) is an important hydrological marker that conveys additional information not captured by precipitation or temperature alone. From the simulations, we use the variables surface temperature, total precipitation amount, and the isotopic precipitation. The drought index SPEI (Standardized Precipitation Evapotranspiration Index Vicente-Serrano et al. (2010)) is computed from simulated precipitation and temperature using the code based on the Thornthwaite's method for estimating potential evapotranspiration from the climate-indices package (Adams, 2017). The time scale is set to 12 months. We choose Thornthwaite's method over the more precise Penman-Monteith formula, because the available climate model simulation data does not include all variables required for the latter. In parts of the analysis, we use a Multi-Model Ensemble (MME) by conducting separate reconstructions for each model prior and then computing the mean of the five reconstructions. In PaleoDA, MMEs are being used to provide more reliable reconstructions than provided by single model priors (Parsons et al., 2021; Annan et al., 2022; King et al., 2021, 2023). As we will use the climate model data only as anomalies, the purpose of the MME in this study is not to alleviate the effect of mean value biases in the models, but to provide a more diverse covariance structure, which constitutes the backbone of the PaleoDA reconstruction algorithm (see Section 3.1). This covariance structure across models is particularly relevant in our study, as the covariance relationships between δ^{18}O and other climate variables as temperature and precipitation vary considerably in the different climate models. An MME requires regridding of all climate model simulations to the same grid. We choose to interpolate all climate model simulations to the highest resolution provided by one of our input models, isoGSM (1.875° x 1.875°). This allows for keeping the spatial information of the higher resolving models. Computing the correlation fields for the regridded climate fields, we found that the regredding produces smoothed correlation fields without introducing artefacts (not shown). Note, that it is also conceivable to construct an MME by concatenating the model priors before applying the Ensemble Kalman Filter equations, but this method is not used here.

Model	Resolution	Reference
ECHAM5/MPI-OM	$3.75° \times 3.75°$	Sjolte et al. (2020) Werner et al. (2016)
GISS ModelE2-R	$2.5° \times 2°$	Lewis and LeGrande (2015) Colose et al. (2016a) Colose et al. (2016b)
iCESM1	$2.5° \times 1.875°$	Brady et al. (2019) Stevenson et al. (2019)
isoGSM	$1.875° \times 1.875°$	Yoshimura et al. (2008)
iHadCM3	$3.75° \times 2.5°$	Bühler et al. (2021) Tindall et al. (2009)

Table 1. Spatial resolutions and references of the isotope-enabled last millennium simulations used in this study. The listed references also include the model descriptions. For a detailed description of boundary conditions and forcing parameters see Bühler et al. (2022).

3 Methods

3.1 Data Assimilation with the Ensemble Kalman Filter as a Climate Field Reconstruction technique

Data assimilation (DA), which has been developed mainly for improving numerical weather and ocean fore- and hindcasts, combines two sets of information: a statistical prior state estimate that is provided by an ensemble of estimates from a nu-
205   merical model, and information from observations (e.g. climate proxy records). The prior estimate is updated conditional on the observations (Evensen et al., 2022). The obtained posterior state is then propagated through time by the numerical model until new observations are available. PaleoDA often simplifies some aspects of DA compared to operational weather and ocean forecasting systems, particularly by omitting the model ensemble restart step due to the limited predictability and the computational cost of General Circulation Models (GCMs) on paleoclimatic timescales (Dirren and Hakim, 2005; Huntley and Hakim,
210   2010). AF B1 illustrates the main steps of the PaleoDA algorithm. Here, the updating operation is performed by the Ensemble Kalman Filter (EnKF) (Evensen, 1994), which assumes that the prior and the observations are sampled from the same true, but unknown Gaussian distribution. The errors with respect to the true distribution are assumed to be unbiased and normally distributed. The EnKF further assumes that the observations are linearly related to the true distribution. Despite the normality assumptions, it has proven to be also a good estimator in non-linear cases where the assumptions do not strictly hold, which
215   explains its wide use in real-word applications (Evensen et al., 2022). In the last decade, the EnKF has been introduced into the field of climate field reconstructions (Bhend et al., 2012; Steiger et al., 2014) and been used to reconstruct the climate of the last two millennia (e.g Hakim et al., 2016; Steiger et al., 2018; Tardif et al., 2019) and older periods such as the Last Glacial Maximum (Tierney et al., 2020; Annan et al., 2022), the last deglaciation (Osman et al., 2021; Erb et al., 2022), and the Paleocene–Eocene Thermal Maximum (Tierney et al., 2022).

220 The EnKF assimilation equation states

$$\mathbf{X} = \hat{\mathbf{X}} + \mathbf{K}(\mathbf{Y} - \mathcal{H}\hat{\mathbf{X}}), \tag{1}$$

where $\hat{\mathbf{X}}$ is the prior state (e.g. a surface temperature field over all simulated time steps, which creates an ensemble) and $\mathbf{X}$ the posterior state matrix. $\mathbf{Y}$ is the observation vector containing the proxy record values at a specific time step and $\mathcal{H}$ is the observation operator mapping the prior values to the observations (further explained in Section 3.3), thus creating $\mathcal{H}\hat{\mathbf{X}}$, the

225 observation estimates for the simulated values. $\mathbf{K}$ is the Kalman gain matrix, a weighting matrix, which blends the prior state estimate and observations according to covariances in the prior ensemble and the proxy record uncertainty. It is computed as

$$\mathbf{K} = \text{cov}(\mathbf{X}, \mathcal{H}(\mathbf{X}))(\text{cov}(\mathcal{H}(\mathbf{X}), \mathcal{H}(\mathbf{X})) + \mathbf{R})^{-1}. \tag{2}$$

$\mathbf{R}$ is the observation error covariance matrix which contains the error associated with the proxy records (see Section 3.4). We assume, that the observation error of different proxy records is uncorrelated, hence $\mathbf{R}$ is a diagonal matrix. The EnKF

230 assimilation equation can be effectively described as an interpolation process, where the model prior provides covariance estimates between observation locations and all simulated locations to perform the interpolation. Equation 2 follows from minimizing the posterior error covariance matrix, which is given by

$$\text{cov}(\mathbf{X}, \mathbf{X}) = (\mathbf{I} - \mathbf{K}\mathcal{H})\text{cov}(\hat{\mathbf{X}}, \hat{\mathbf{X}}). \tag{3}$$

The uncertainty of the reconstructed variables at each time step can be computed as the standard deviations of the diagonal

235 entries of the posterior error covariance matrix (Equation 3). The posterior covariance matrix is by construction less than or equal to the prior covariance. To solve the equations 1, 2 and 3 efficiently, we utilize the Ensemble Transform Kalman Filter (Bishop et al., 2001) as formulated in Vetra-Carvalho et al. (2018). The prior covariance matrix $\hat{\mathbf{X}}$ is used from already computed simulations instead of restarting the model ensemble and thus represents the climatological covariance. To compute it, we use an ensemble of 100 randomly selected simulation years (see Section 3.5). This approach has been named stationary

240 offline PaleoDA (Okazaki et al., 2021) and assumes a stationary covariance between climate variables at the grid cells. Each year is reconstructed separately, with the temporal pacing determined by the climate proxy records and the spatial information provided by the covariances from the climate model simulations. Note, that by using an MME (Section 2.2), we effectively use the mean Kalman gain from the five model priors. The offline PaleoDa concept is similar to computationally efficient Optimal/Statistical Interpolation methods (Evensen, 2003; Oke et al., 2005), although these still forward a single model simulation

245 in time according to the results of the assimilation.

We reconstruct both annual (April-March, according to the vegetation cycle) and austral summer (DJF) means separately, due to the selected proxy records likely representing either annual or summer means (in particular speleothems from the SASM region).

In our reconstruction, the prior ensemble mean for each grid cell and climate variable is always enforced to be zero to limit

250 model mean value biases. We consider this a valid approach, as the CE is a relatively stable climatic period. Not performing such debiasing would introduce steplike, unphysical shifts in the reconstructed time series depending on the availability of specific proxy record with a strong difference towards the prior (as also noted in Franke et al. (2017) for example).

3.2 Multi-time scale Paleoclimate Data Assimilation

The PaleoDA algorithm described in the Section 3.1 is usually employed for the assimilation of proxy records at a single time scale, e.g. annual or seasonal for the CE. However, the speleothem records that are the backbone of our regional reconstruction have median temporal resolutions of 1 to 8 years and actually represent smoothed climate signals due to mixing effects of the karst system on the cave drip water (Moquet et al., 2016). Therefore, we developed a new multi-time scale adaptation of the EnKF-PaleoDA algorithm, building on the concept proposed by Steiger and Hakim (2016), which allows us to use low- and high-resolution proxy records simultaneously in a computationally efficient manner.

The key idea is to add an additional time dimension for consecutive years in the prior state matrix $\mathbf{X}$, enabling the use of multi-year means and covariances in the PaleoDA algorithm (see AF B2). The number of years added in the prior state matrix is determined by the largest time scale imposed by the proxy records, which we determine as decadal for the employed speleothems. Instead of reconstructing the target time period (1-2000 CE) year by year, we divide it into decadal blocks, as we will use the speleothem values on a decadal time scale only. Additionally, we reconstruct annual and quinquennial time scales as sub-blocks of the decadal block (see AF B3). The decadal prior block is the same during the entire reconstruction period. For each decadal block, the algorithm computes the assimilation equations for all proxy records that represent the largest time scale, using decadal means in the prior state matrix. The resulting decadal mean value is then exchanged in the prior state matrix. The algorithm continues with the smaller time scales using the corresponding proxy records. Each proxy record is used on a single time scale. This procedure requires resampling the records to the target resolution of the desired timescale prior to the Data Assimilation. We first bin all the non-annual proxy records to the respective resolution using a simple equidistancing resampling routine, which consists of upsampling the time series values to annual resolution, filtering the time series with a low-pass filter and finally resampling to the targeted resolution (similar to the `MakeEquidistant` function of the Paleospec R package (Laepple et al., 2023a)). We ensure the resampling does not add spurious datapoints by choosing target resolutions that are larger than the largest proxy record sampling interval and mask longer gaps in the proxy records. The multi-time scale algorithm involves more calculation steps than the single-time scale algorithm due to the repeated calculation of multi-year means and anomalies in the prior state matrix. As such, the algorithm also requires the repeated application of the observation operator $\mathcal{H}$ in the Kalman Filter equations. However, this is avoided by appending the observation estimates to the prior state matrix, such that the algorithm also updates the observation estimates. A multi-time scale paleoclimate data assimilation approach is not only advantageous to allow for the assimilation of irregular proxy-records, it should also improve the reconstruction of multi-decadal to centennial climate variability according to pseudoproxy experiments (Steiger and Hakim, 2016; Choblet et al., 2023). Note, that this multi-time scale PaleoDA algorithm differs from the one used in the Holocene temperature reconstruction by Erb et al. (2022), where the multi-time scale prior ensemble is constructed as a moving prior ensemble from transient climate simulations.

3.3 Proxy system models

In PaleoDA, Proxy System Models (PSM) (Evans et al., 2013; Dee et al., 2015) are employed for the observation operator $\mathcal{H}$ in equation 1 and 2. They have been developed to enhance model-data comparison by encapsulating the physical, geological, biological and biogeochemical processes into mathematical formulas to translate the external climatic conditions into a proxy record signal. These processes are usually divided into three different stages, the sensor, archive and observation stage. In this study, we use PSMs in a one-stage manner, which is commonly chosen in PaleoDA studies targeting the CE climate (e.g. Hakim et al., 2016; Steiger et al., 2018; Tardif et al., 2019). Within this PaleoDA study, the PSMs translate the signal of simulated climate to proxy record units (the proxy record variance), accounting for seasonality. We employ three types of PSMs depending on the nature of the proxy records:

A) For records already calibrated to temperature, such as some lake and marine sediments and sclerosponges, the PSM takes the temperature of the model grid box closest to the proxy record location as the simulated temperature value. Seasonal means or annual means (April to March) are used depending on the indications in the original publication of the record. This way, seasonal biases in the reconstruction are constrained.

B) For proxy records that reflect changes in δ^{18}O of precipitation, such as speleothems, ice cores, and some lake sediments, the PSM uses the simulated δ^{18}O of precipitation values from the closest locations to the proxy records. Annual means of precipitation-weighted δ^{18}O values are computed to account for varying precipitation intensity over the year. The values of the two ice core records given in deuterium are divided by 8 to represent the variability in δ^{18}O according to the Global Meteoric Water Line (Craig, 1961). Although the δ^{18}O values in these different archives is stored in different materials (e.g ice, carbonates, trees) and, thus, have different mean values, this is not relevant for our reconstruction, because we use proxy record anomalies respective to a reference period. We assume that temperature dependent fractionation effects are small compared to the variation in the δ^{18}O of precipitation values.

C) For proxy records that can be calibrated to instrumental data, such as corals, tree rings and documentary indices, we employ a linear regression- based PSM as usually employed in PaleoDA (e.g. (Hakim et al., 2016; Steiger et al., 2018; Tardif et al., 2019; King et al., 2021; Sanchez et al., 2021; Valler et al., 2024). While more specific PSMs for corals and tree rings exist, the linear-regression based PSMs also yield similar reconstruction results in PaleoDA (Dee et al., 2016). More complex PSMs for corals and tree rings also require environmental variables for sea water and air moisture, which are not available for all employed climate model simulations. Furthermore, we consider it preferable to use this type of univariate linear PSMs in PaleoDA, as the covariance relationship between observations and reconstructed climate field remains more tractable. Linear regression equations are estimated between the proxy time series and instrumental time series over a calibration period. The regression parameters are then applied to the model data in the data assimilation. Different predictor variables, such as surface temperature, precipitation, or the SPEI drought index, are used based on the lowest p-value for each proxy record. For coral records, we only use surface temperature as a predictor variable. As instrumental calibration datasets, we use the Berkeley Earth dataset for surface temperature (Rohde and Hausfather,

2020), precipitation from CRUTS 4 (Harris et al., 2020b) and an SPEI drought index computed from the temperature and precipitation in CRUTS 4. The temperature calibration is performed over the period 1920 - 2000 CE. For precipitation and SPEI, we use the period 1950 - 2000 CE due to limited local station data in South America before 1950 CE (Garreaud et al., 2009). These spatially highly resolved instrumental datasets have been regridded to the spatial resolution used in the climate field reconstruction to account for the lower spatial resolution of the climate model simulation data. We compute these regressions both for the annual and seasonal instrumental means and choose the best predictor variable separately (as in Steiger et al., 2018). For the annual reconstruction, 110 tree-ring records were predicted with temperature, 94 with SPEI and 51 with precipitation. One historical documentary records was predicted with temperature, four with SPEI and nine with precipitation. For the austral summer reconstruction, 102 tree-ring records were predicted with temperature, 92 with SPEI and 61 with precipitation, whereas two historical documentary records were predicted with temperature, six with SPEI and three with precipitation.

3.4 The proxy record error

The proxy record error in Data Assimilation represents the non-climatic noise recorded by proxy records and is challenging to quantify. Measurement noise is considered negligible. For the tree, coral and documentary archives, where calibration could be performed with instrumental data, the proxy error follows directly from the linear regression in the PSM (See Section 3.3). The mean of the squared linear regression residuals is the proxy error variance. For all other records in the non-instrumental era, we express the proxy record error in terms of the signal-to-noise ratio (SNR), assuming Gaussian and timescale-independent noise (Smerdon, 2012). We assume an SNR of 0.5 for all proxy records which we have not calibrated to instrumental variables, following exploratory studies by Wang et al. (2014) and Orrison et al. (2022).The SNR can then be converted into the entries of the observation error matrix $\mathbf{R}$ in Equation 2 by taking into account the variance of the proxy records, var($\mathbf{Y}$), (see Appendix B1 for the derivation):

$$\mathbf{R} = \text{var}(\mathbf{Y})/(1 + \text{SNR}^2) \tag{4}$$

$\mathbf{R}$ is computed for each proxy record that can not be calibrated using its resampled time series (see Section 3.2). Given that some proxy records, particularly speleothems, exhibit significant shifts in local climate or environment, we observed that the variance and thus $\mathbf{R}$ would be larger compared to those not indicating such local changes. Consequently, the former records exerted less influence during the reconstruction. To address this issue, we used the mean of the variance in a running 200-year window for computing var($\mathbf{Y}$) to reduce the influence of shifts on the variance and to ensure comparable noise levels for all proxy records. We thus assume, that for a 200 year window, the statistical assumptions of Gaussian and timescale-independent noise leading to equation 4 hold. We emphasize that the proxy record error should not be considered separately from the variance in the prior ensemble matrix, which represents the model error (see Equation 1). The relationship between proxy error and prior variance is crucial in PaleoDA. While in regular Data Assimilation via the optimal interpolation method, the static prior variance is usually considered to be too large and thus reduced by a factor (e.g. Oke et al., 2005), climate simulations have been allegedly underestimating climate variability, for instance in surface temperature (Laepple and Huybers, 2014; Laepple

350 et al., 2023b) or isotopic variability in precipitation (Bühler et al., 2022), which could be used as an argument in favor of inflating the variances in the prior. Instead of adjusting the variance in the prior, we also performed alternative reconstructions in which the proxy error variance for non-calibratable records was set equal to the variance in the prior observation estimates. This approach gives equal weight to the proxy observations and the model prior.

3.5 Further reconstruction refinements

355 We use a Monte Carlo technique of repeating the reconstructions 50 times with different ensembles of 100 randomly selected simulation years and using 80% of all proxy records in each repetition similar to Hakim et al. (2016) and Tardif et al. (2019). Doing so improves the representation of the reconstruction uncertainty, attenuates the effect of outliers in the proxy record selection and the prior ensemble provided by the climate model simulations as suggested by Pseudoproxy Experiments. The withheld proxy records will be used for internal validation of the reconstruction. Covariance localization, which is used to
360 suppress spurious long range covariances is not employed in this study, because the prior ensemble size is considered large. Furthermore, PaleoDA studies that use covariance localisation usually do so with very large decorrelation lengths larger than 12000 km (e.g. Tardif et al., 2019; Tierney et al., 2020; Osman et al., 2021), exceeding the targeted area in our reconstruction.

4 Validation

We validate our reconstruction using gridded instrumental data sets from the 20th century, independent reconstructions and
365 proxy records withheld from the reconstruction. The focus here is put on the internal validation using withheld proxy records as performed in previous PaleoDA studies (e.g. Tardif et al., 2019; King et al., 2021; Tierney et al., 2020; Osman et al., 2021). The reason for doing so is that although instrumental validations are commonly used in PaleoDA and most easy to interpret, we do not consider them representative in our case due to the shortness of the instrumental record compared to our decadal and quinquennial climate archives. The instrumental temperature and precipitation time series are too short for validating a
370 decadal-scale reconstruction. The 20th century validation mainly reflects the reconstruction capability of tree rings, which are the most abundant climate archive in the instrumental period but only provide limited spatial and temporal coverage during the entire CE. The inclusion of speleothems in this study mainly relies on the assumption that their δ^{18}O signatures capture monsoon variability, locally validated in Moquet et al. (2016) and Jiménez-Iñiguez et al. (2022). Correlation analysis of the model data supports, that this assumption is conveyed in our reconstruction. An extensive validation using gridded instrumental
375 temperature and precipitation data for evaluating the reconstruction regionally and for the SASM precipitation amount is presented in Appendix C1 and C2. A validation of the reconstructed drought index for the Southern Cone, for which independent reconstructions exist is presented in Appendix C3.

Withholding proxy records in each repetition of the repeated Monte Carlo reconstructions allows us to perform an internal
380 validation of the reconstruction (see Section 3.5). The proxy record estimates from the simulation data (e.g. the simulated isotopic composition of precipitation of the grid cell in which a cave is located) are still part of the prior state matrix, also
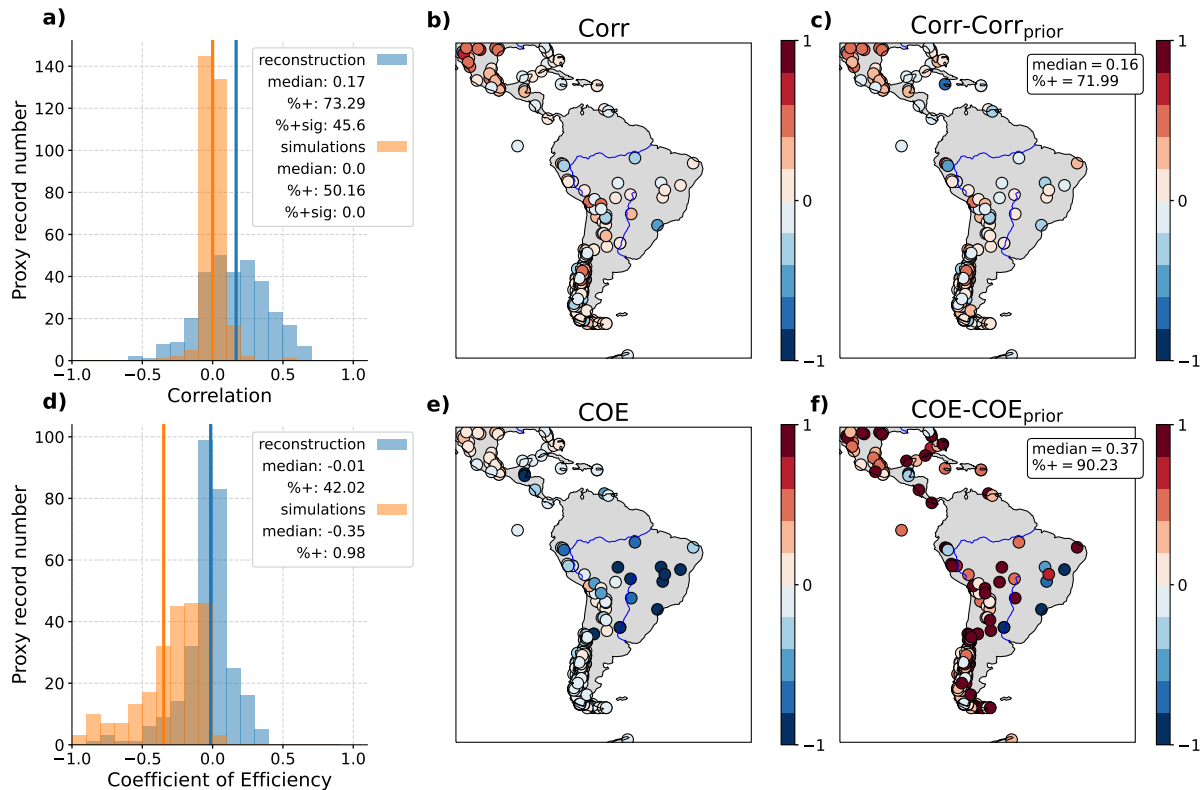
Figure 2. Internal validation. We compute the correlation (a,b,c) and Coefficient of Efficiency (COE) (d,e,f) of reconstructed proxy record time series to true proxy record timeseries when the proxy records are not used as input data in the reconstruction (withheld proxy records). Panel a) and d) show the histogram of the skill scores. The box in the upper right corner displays the median value, the percentage of positive values (%+) and the percentage of positive and significant correlations (%+sig, p-value < 0.05) for the distributions. Panels b) and e) display the skill scores for each location. We additionally computed the skill scores for the model simulations (mean of the five models for each proxy record), which are also included in the histograms and used for a comparison between reconstruction skill scores and the model simulations (c,f). Note, that the COE can also take values smaller than -1. In effect, 25% of the COE values for the simulations fall outside of the histogram. While all colorbars have been limited to the range (-1,1) for clarity, values in e) and f) can be more negative than -1, and the difference between reconstruction and simulations in f) also larger than 1.

when a proxy is not used as input data and, therefore, updated in the PaleoDA algorithm. We calculate the correlation and Coefficient of Efficiency (COE) (Nash and Sutcliffe, 1970) of the withheld proxy record time series to their reconstructed counterparts. While the correlation rewards a correct timing of the reconstructed values, the COE is also sensitive to bias and errors in the amplitude by taking into account the variance of the true signal. The COE can take values in the range $[-\infty,1]$, with positive values indicating skill. However, as pointed out by Cook et al. (1999) and Hakim et al. (2016), the coefficient of efficiency (COE) can misleadingly yield negative skill scores due to proxy records and reconstructions having different mean values and thus the comparison to the prior can be more meaningful than the absolute skill scores. We therefore also compute

385

these scores for the prior model simulations and compare the obtained values to those of our reconstruction. To enable a fair comparison between model priors and reconstructions, the skill scores are computed for the period 850-1850CE, which is the period covered by the model simulations. The correlation and COE are computed as the mean correlation for all Monte Carlo repetitions in which a proxy record is not used, by resampling the reconstructed time series to the respective temporal resolution of each proxy record. As we performed 50 Monte Carlo reconstructions with 20% of withheld proxy records, there are on average 10 reconstructions for each proxy record for which it has not been used as input data. This allows us to assess if the reconstruction is in accordance with independent proxy record data and indirectly identify regions in which proxy data share a common climate signal and are similarly reconstructed. The results are displayed in the form of histograms and on maps in Figure 2.

We obtain predominantly positive correlations (73.29%), with a median value of 0.17. Almost half of the correlations are positive and significant (45.60%). As the correlations of the model simulations to the proxy records are negligible, the reconstruction does lead to a clear improvement in correlation with a median increase of 0.16 and 71.99% of the records with an improvement. However, a few records stand out with negative correlations in the reconstruction, particularly in geographically isolated areas, while higher correlations are generally obtained in regions with numerous proxy records. For the COE, the obtained median value is -0.01. Yet, 42.02% of the values result in a positive COE. In comparison to the model priors, there is a notable median increase of 0.37, with 90.23% of records demonstrating an improved COE value and thus skill of the reconstruction.

The COE score results underscore the high dissimilarity of proxy records in northern and eastern Brazil, possibly linked to the climate dipole between northeastern Brazil and the core SASM region (Novello et al., 2018; Campos et al., 2019; Wong et al., 2021), where speleothem records exhibit opposing δ^{18}O trends. This spatial homogeneity in the reconstruction may potentially mask this crucial feature of South American climate. Such homogeneity is expected due to the coarse model grid resolution and the spatial smoothing of the EnKF based reconstruction method, in contrast to the high spatial variability of the proxy records. While the absolute skill values appear low, they are comparable to those obtained in the global multi-proxy reconstruction by Hakim et al. (2016); Tardif et al. (2019); King et al. (2021). The comparison to the skill scores of the prior model simulations emphasizes that the assimilated product represents the climate signal of the proxy records better.

5 Results

5.1 Centennial climate changes

Having examined the potential and limitations of our algorithm we now examine the climatic features displayed by the reconstruction. As a first application, we analyze the newly reconstructed climate anomalies during the MCA and the LIA. The definition of these anomalous climate periods is equivocal, as they have not occurred synchronously globally (Neukom et al., 2019). Therefore, we decide to examine finer intervals, namely the period preceding the MCA (Pre MCA, 700 - 925 CE), the Early and Late MCA (925 - 1150 CE, 1150 - 1350 CE) as in Azevedo et al. (2019), a transition period (Trans, 1350 - 1500 CE), the LIA (1500 - 1850 CE), and also the current warm period (CWP) (1900 - 2000 CE) to put the anomalies into
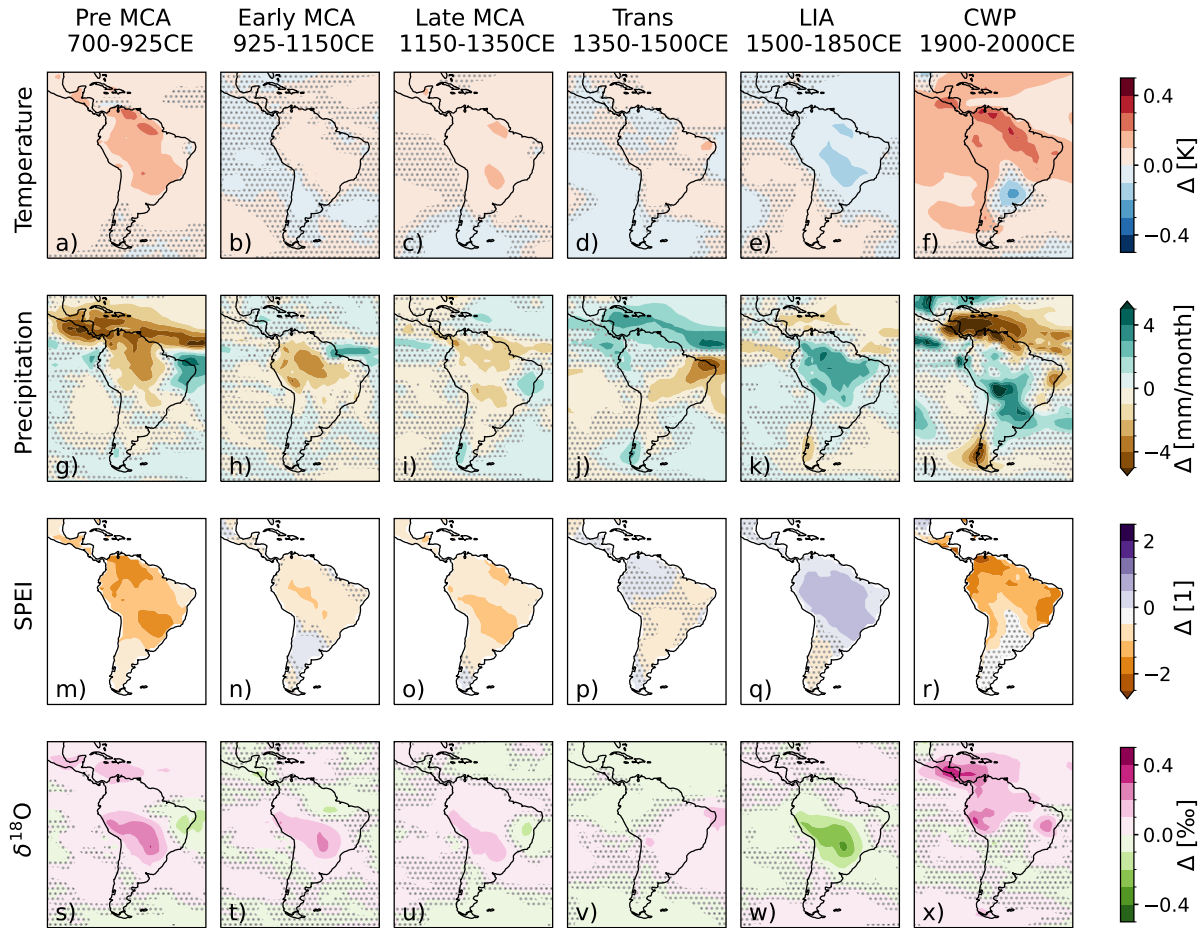
Figure 3. Reconstructed mean anomaly fields for temperature (a-f), precipitation (g-l), SPEI (m-r) and δ^{18}O (s-x) during five periods with respect to the Last Millennium mean (LM, 850 - 1850 CE). The studied periods are the years preceding the Medieval Climate Anomaly (Pre MCA, 700-925 CE, first column), the early MCA (925-1150 CE, second column), the late MCA (1150-1350 CE, third column), the transition period (Trans, 1350 - 1500 CE, fourth column), the LIA (1500 - 1850 CE, fifth column) and the current warm period (CWP) (1900-2000 CE, sixth column). The SPEI values have been standardized using the variance of the period 850 - 1850 CE. Stippling indicates grid cells where the difference to the Last Millennium values is not significant according to a Welch's t-test ($\alpha > 0.01$).

context. Figure 3 shows the anomalies for the annual reconstruction with respect to the mean of the last millennium (LM, 850 - 1850 CE). The same figure for austral summer (DJF), which overlaps with the monsoon period is displayed in AF D1 and for the alternative proxy error definition in AF D2. For the precise temporal evolution of the reconstructed variables, the reader is referred to video supplement 1. The reconstructed patterns are mostly homogeneous over the continent and show a trend towards colder and wetter conditions during the LIA, especially for the central and northern part of the continent. The Southern Cone, however, experienced warmer and drier conditions during the LIA. Warmer and drier conditions are predominant during the transition period, in particular preceding the MCA, except for the Southern Cone and the Nordeste (North Eastern Brazil). In the reconstruction using the equal variance proxy error definition (AF D2), trends with similar pacing are observed, yet exhibiting greater strength. Remarkably, the important changes of the hydroclimate state before the CWP are mostly conveyed by the speleothem proxy record information, as reconstructions relying only on speleothem data and without speleothem data reveals (AF D3 and AF D4).

We observe in-phase trends for all reconstructed climate variables and studied periods, generally indicating a simultaneous occurrence of warmer with drier conditions and colder with wetter periods, except during the CWP. Compared to the last millennium mean, the reconstructed CWP anomalies show a more spatially diverse precipitation anomaly field with increased precipitation for the center of the continent. Less precipitation is reconstructed for coastal locations in the north, east, and southern margins of the continent. Temperature and SPEI, in contrast, show warmer and drier conditions for the entire continent, except parts of the La Plata basin and parts of the Southern Cone. The austral summer reconstruction (AF D1), however, shows the largest positive temperature anomaly for the Southern Cone. For both annual and austral summer reconstructions, the 20th century is warmer and drier than all preceding phases. In terms of spatial homogeneity, the temperature and SPEI anomalies are more extensive compared to the precipitation reconstruction, which has more diverse spatial features. The reconstructed δ^{18}O of precipitation values for the studied periods change most in the center of the continent, with a trend towards most depleted precipitation during the LIA. The center of the largest changes in the isotopic composition of precipitation is located further to the south than the region of the largest precipitation changes. The δ^{18}O values of precipitation display a dipole pattern over the Nordeste and central South America, except during the more homogeneous MCA-LIA transition period and CWP, where a pronounced δ^{18}O enrichment is seen for the northern and western part of the continent.

5.2 South American Summer Monsoon variability

To assess changes in the SASM strength throughout the past two millennia, we analyze the mean precipitation anomaly in the core monsoon region as a simplified monsoon index. We use the definition by Vuille et al. (2012), who proposed computing the mean precipitation in the core monsoon region (5° S–17.5° S/72.5° W–47.5° W, see black rectangle in Figure 1) as an indicator of monsoon strength. Additionally, we further investigate δ^{18}O, temperature and SPEI changes in the core monsoon region. Figure 4 shows the anomalies from the annual reconstructions in comparison to the reconstructions LMRv2.1 (Tardif et al., 2019) and PHYDA (Steiger et al., 2018). We also performed the reconstruction with subsets of the complete proxy record database, only relying on speleothems or tree data, or excluding the speleothems from the complete proxy record database to investigate the effect of using different climate archives.
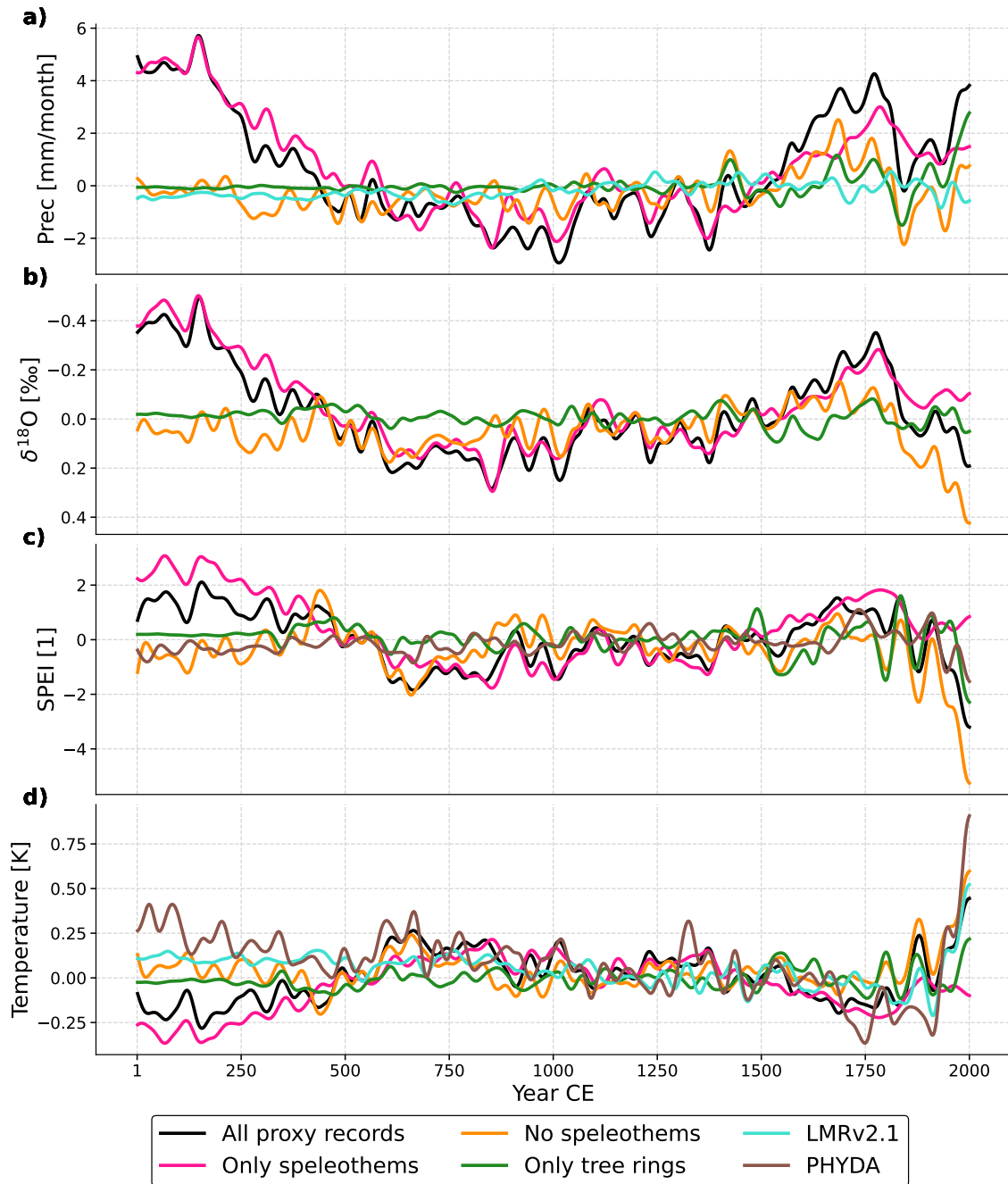
Figure 4. Mean anomalies of precipitation, δ^{18}**O , SPEI, and temperature in the core monsoon region** $(5° − 17.5°$ S / $72.5° − 47.5°$ W). Comparison of reconstructed mean annual precipitation (panel a), δ^{18}O (panel b), SPEI (panel c) and temperature (panel d) anomalies in the core monsoon region from reconstructions using all proxy records, excluding the speleothems, using only speleothems and only trees and the reconstruction products PHYDA (Steiger et al., 2018) and LMRv2.1 (Tardif et al., 2019). All time series have been smoothed with a 50-year-lowpass-filter. The anomalies are displayed with respect to the 850 - 1850 CE mean. Note the inverted y-axis for δ^{18}O in order to match the precipitation trend. PHYDA and LMRv2.1 do not include all variables studied here, and are thus partially missing in panel a), b) and c). The SPEI values have been standardized using the variance of the 850 - 1850 CE period. For means of comparability between different reconstructions, we have chosen to display the annual mean reconstruction.

Overall, the reconstructed monsoon index in Figure 4 and the video supplements 2 and 3 show a colder and wetter LIA, particularly after 1500 CE with anomalies of up to 4 mm/month in the lowpass-filtered curve. Least precipitation is reconstructed for the period from 750 - 1100 CE, while the SPEI values reach a local minimum earlier in the period 600 - 900 CE, and thus seem to more strongly follow the temperature curve, which reaches a local maximum during the same period.

460 Reconstructed temperatures are highest and SPEI - SASM indices lowest during the 20th century. This hints at the effects of anthropogenic warming being evident in the core monsoon region on a centennial time scale. Figure 4 shows that the tree-only reconstruction does not reflect the pronounced centennial hydroclimate variability, although the tree ring data represents the dominant climate archive in our proxy record database in terms of numbers. Comparing the reconstruction that exclusively uses speleothem records to the one that excludes speleothems reveals reconstructed hydroclimate changes in the core monsoon

465 region to be largely driven by the speleothem signal. However, wetter LIA conditions are also captured by other archives. The same figure for the austral summer reconstruction and the *all proxies* estimates can be found in AF D5, exhibiting similar trends but larger magnitudes. Furthermore, the smaller reconstruction uncertainty for reconstructions involving speleothems is noticeable, especially compared to the tree ring only reconstruction prior to 1400CE (AF D6), although the overall uncertainty remains large due to the large spread in the prior ensemble.

470 Figure 4a additionally displays the LMRv2.1 precipitation reconstruction, which shows lower centennial-scale variations, including no significant changes during MCA, LIA or CWP. Precipitation is not included in the PHYDA reconstruction; however, the comparison of reconstructed SPEI also presents less hydroclimate variability during the LIA and the pre and early MCA phase. The temperature reconstruction in Figure 4c shows the largest range of values for the PHYDA reconstruction, followed by the reconstructions of this study, and lastly the LMR reconstruction, which shows the least temperature variability.

475 PHYDA shows a constant temperature decline during the CE with a steep reversal during the 20th century, resulting in the expected hockey stick-like curve, which is also found in our reconstruction, except before 400 CE. The period before 400 CE is peculiar for our reconstruction in all four variables. It shows very wet and cold conditions for the first two centuries of the CE and a subsequent transition to more neutral conditions. The reconstructed extremes even exceed the LIA in magnitude.

We note that the presented results draw on mean values of the MME reconstruction. As visible in Figure 5 for the precipi-

480 tation and AF D7 for all reconstructed variables, the magnitude of reconstructed changes can vary considerably between the single model reconstruction. It is noticeable, that the prior to 400CE wet phase is particularly pronounced in the isoGSM and ECHAM5 model, and is only wetter than the LIA in these two models. For the austral summer SASM index reconstruction (AF D5), the range of values for the precipitation anomalies is almost twice as large as for the annual reconstruction, although the overall trends are very similar. Comparing the all proxy record reconstruction to the prior model simulation without PaleoDA

485 shows that while the model simulations do exhibit more important fluctuations, they do not exhibit clear trends, for instance of a cooler and wetter hydroclimate during the LIA (AF D8).

To further study and quantify climate variability in the core monsoon region we calculated the power spectral distributions of the precipitation anomaly curves (Fig. 6a). In addition, the continuous wavelet spectrum of the SASM precipitation reconstruction involving all proxy records was computed to investigate the power variation in time over the common era (Fig. 6b). The

490 same spectral analysis for the reconstructed δ^{18}O signal in the core monsoon region can be found in AF D9. The precipitation
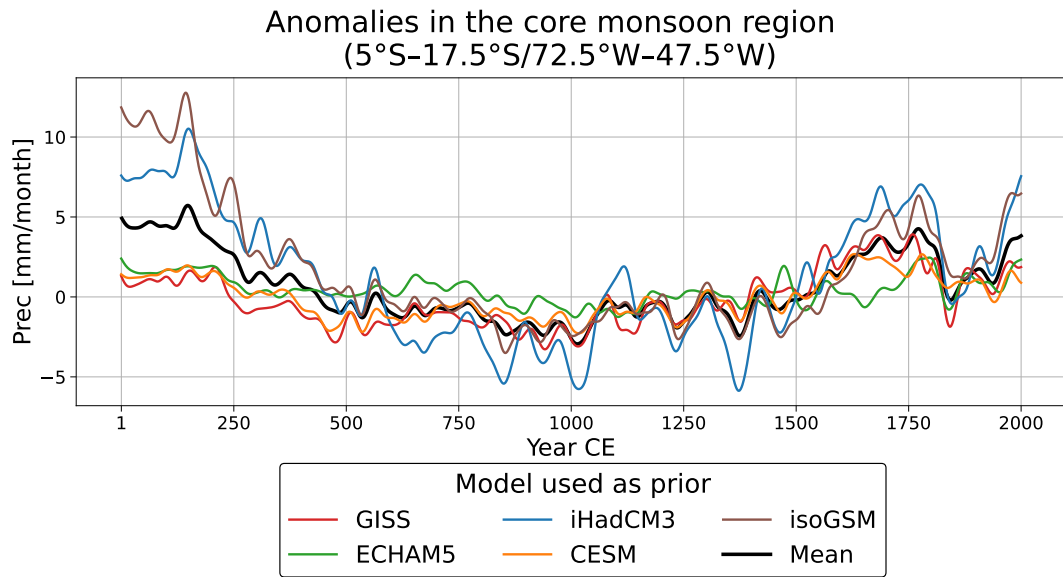
Figure 5. Single model reconstructions of the monsoon precipitation index using all proxy records, highlighting the prior dependency of the precipitation reconstruction. The black line denotes the the multi-model mean, which is used in the multi-model ensemble analysis.
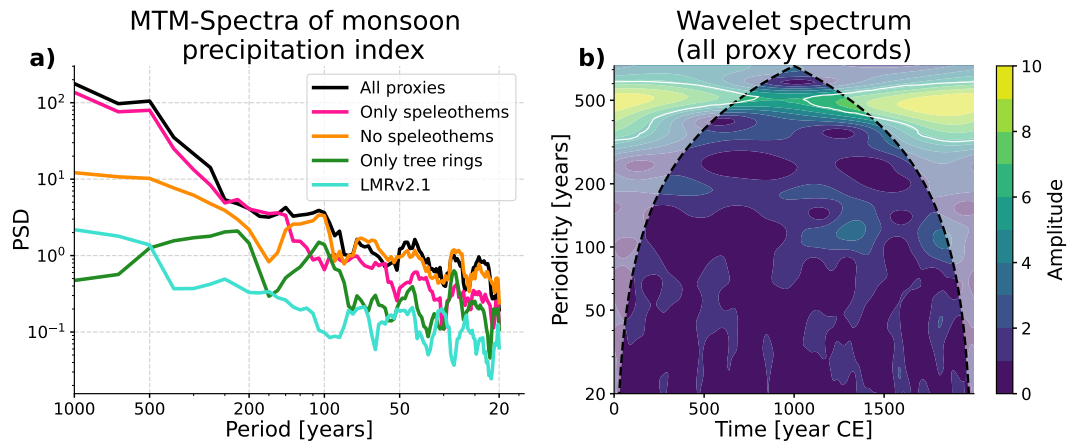
Figure 6. Spectra of reconstructed monsoon precipitation index. On the left (a), the Multitaper method (MTM) - power spectral densities (PSD) of the annual reconstructions involving different subsets of the proxy record database. The time series have not been standardized and detrended, but resampled to 10 year averages to achieve comparability between reconstructions involving different time scales. On the right (b), the continuous wavelet spectrum for the reconstructed time series involving all proxy records is shown. The dotted black line indicates the cone of influence and the white lines indicate the 95% significance level for an AR1 process. All spectra have been computed using the Pyleoclim package in Python (Khider et al., 2022).

spectra have typical *red noise* characteristics, with the power decreasing exponentially towards higher frequencies, except for the reconstruction only based on tree data, which has a flat power spectrum. The reconstructions including the speleothems show the highest redness with a decline in power over three orders of magnitudes, as also indicated by the pronounced multi-centennial variability in Figure 4. Without the speleothems, the power distribution extends over two orders of magnitude. The power spectrum of the SASM precipitation anomaly in the LMRv2.1 reconstruction, remains flat and similar to the spectrum of the tree-ring only reconstruction. The wavelet spectrum of the all proxy precipitation reconstruction also exhibits multi-centennial variability of the SASM (Fig. 6b), although it is not above the signfance threshold. The spectra for the δ^{18}O-SASM index, which might be represented more directly by the available proxy records show similar *red noise* characteristics (AF D9). For further comparison, we compared the spectrum of the SASM precipitation index to the spectra of the index in the prior model simulations. To do so, we took into account that the model simulations span a shorter time period than the entire reconstruction period and that they have a higher variance than the reconstruction. The spectra of all five model simulations have a flat shape and thus a smaller variability scaling than the reconstruction (AF D10).

6   Discussion

6.1   Reconstructed hydroclimate changes

Our climate field reconstruction of the South American Hydroclimate during the CE represents a comprehensive synthesis of an encompassing diverse collection of proxy record data and isotope-enabled climate simulations. The reconstructed centennial climate changes in tropical South America, transitioning from a drier MCA to a wetter LIA, align well with individual proxy record assessments from the region (Bird et al., 2011; Vuille et al., 2012; Deininger et al., 2019) and proxy record syntheses (Campos et al., 2019; Orrison et al., 2022). The consistency with the conclusions of these studies is expected, given that we used the same (and more) proxy records and the temporal pacing of the reconstruction relies on the information provided by the proxy records within the offline PaleoDA algorithm. We did not perform direct quantitative comparisons between our climate field reconstruction and individual proxy records from single or multi-proxy studies. This is because speleothem δ^{18}O values, being a proxy for large-scale regional atmospheric behavior, is not expected to agree precisely with local hydrology. Our reconstruction aims to capture broader regional patterns rather than exact local conditions.

The PaleoDA climate field reconstruction offers the advantage of extrapolating proxy record information to more climate variables, such as temperature from speleothem δ^{18}O for instance, which in this region is mainly only interpreted in terms of precipitation amount changes. The magnitude of reconstructed precipitation amount and SPEI surpass the estimates from the PHYDA and LMRv2.1 reconstructions, while the changes in temperature show similar magnitudes. It is worth noting that the highest temperature anomalies are reconstructed for the period preceding the MCA reference period 950 - 1250 CE (Fig. 6). This pattern is also observed in the PHYDA and LMR reconstructions (AF D11 and AF D12), which rely on fewer local proxy record data points from South America for that period. In line with Neukom et al. (2019), South America does not show coherent warming during the MCA compared to other regions globally, which contrasts with the qualitative study by

Lüning et al. (2019). Although our reconstruction includes anomalous conditions, their timing might differ from the Northern Hemisphere anomalies. Thus, this reference time period should be used with caution in global comparisons.

525   Another similarity between our reconstruction and PHYDA and LMRv2.1 is the presence of anomalies of opposite signs in the Southern Cone region compared to the Northern and Central part of the continent. The influence of the Southern Annular Mode in this region may, for instance, cause this distinct opposite climate system. Our reconstruction also reveals a spatial feature over northeastern Brazil, where opposite anomalies in precipitation, drought index and δ^{18}O are observed compared to the rest of tropical South America. This dipole pattern, previously identified in regional speleothem studies, has been linked to

530   meridional changes in the Hadley cells (Cruz et al., 2009; Novello et al., 2012, 2018) and interhemispheric temperature gradients (Campos et al., 2022). The presence of this dipole pattern in our reconstruction was not necessarily expected, considering the limited number of speleothems from the Nordeste and the relatively coarse spatial resolution of the climate models. In addition, looking into the spatial correlations of the mean δ^{18}O of precipitation values for that region in the model simulations only shows a dipole in two out of the five climate model simulations (AF D13), thus revealing the benefit of combining proxy

535   and model data with PaleoDA. However, more research for quantifying the extent and possible spatio-temporal variations of the South American δ^{18}O and precipitation dipole is required, also by incorporating additional proxy records from NEB as we currently only employ two.

       A consistent pattern in our hydroclimate reconstruction are the synchronous trends for all variables during most of the CE, except for the 20th century. However, it is essential to acknowledge that the reconstruction technique may also influence this in-

540   phase relationship. Offline PaleoDA with the EnKF, being inherently linear, employs the same static covariance patterns from the simulations at each time step. The in-phase relationship represents the default state of the reconstruction. The increased strength of the SASM during the LIA has been explained by cooler temperatures on the Northern Hemisphere, resulting in a southward shift of the ITCZ (Deininger et al., 2019; Vuille et al., 2012). Integrating our employed proxy records into a global climate field reconstruction, and possibly including more atmospheric variables, could provide a more in-depth understanding

545   and allow for testing this hypothesis.

       An unexpected finding in our reconstruction is the evidence of wetter and colder conditions prior to 400 CE. Primarily, the speleothem data support these changes. Upon closer examination of the individual anomalies of the available records in AF D14, only three records exhibit particularly negative δ^{18}O anomalies for that period. Furthermore, during that time, proxy records from the margin and outside the core monsoon region are the only available sources. Still, the spatial correlations in

550   the model simulations for the precipitation in the core SASM region prove to be extensive, such that the signal from proxy records outside of the region can influence the reconstructed SASM precipitation (AF D15). The increased SASM strength stays consistent even after excluding possibly diverging single records that were suspected to cause the anomalies in the reconstruction.

       While the magnitude of the wet conditions also proved to be model prior dependent, the source of model differences in the

555   reconstruction cannot be directly deduced from the simulated SASM indices and the correlations in the model, requiring further analysis of the topic. In addition to the correlation analysis that we did for the core monsoon region and NEB, an optimal sensor

placement analysis as performed by Comboul et al. (2015) and King et al. (2023) could give insights into how different proxy records influence the reconstruction depending on the model prior.

6.2 Examining reconstructed trends in relation to single proxy records

560 Putting attention to particularly anomalous proxy records reveals further insights into the nature of our reconstruction. For instance, the record with the strongest negative anomaly from Paraiso Cave (SISAL-ID 424) in the eastern Amazon basin (Ward et al., 2019; Azevedo et al., 2019) exhibits a distinctive increase in $\delta^{18}O$ values after 900 CE, resulting in negative $\delta^{18}O$ anomalies during the early Common Era compared to the reference period (1750-1850 CE). This increase may be caused by non-climatic influences, which potentially introduces artifacts in our anomaly reconstruction. The record also stands out in
565 the internal validation procedure (Figure 2). Nonetheless, this record has been cross-validated with archaeological evidence from the region, which also suggests a shift from wetter conditions in the first millennium to drier conditions in the second millennium (de Souza et al., 2019). In contrast to other speleothem locations in tropical South America, the Paraiso Cave record is additionally influenced by the rainfall of the two distinct systems, SASM and ITCZ. Our PaleoDA approach may not be able to resolve this complex local climate. Different to the drier conditions recorded in Paraiso Cave (Ward et al., 2019),
570 the reconstruction does not show drier conditions during the LIA for the eastern Amazon basin, but wetter conditions as for entire tropical South America. While this record has an important influence in the first centuries of the reconstruction, it is outweighed by the multitude of other records during the LIA.

The contrast between reconstructed wetter and colder climate anomaly fields during the LIA to the information provided by single records highlights the spatial smoothing caused by the PaleoDA method, which we consider the central limitation
575 of our study. The EnKF employs spatial covariances between grid cells and variables in the climate model simulations, which tend to be spatially extensive when computed over the last millennium. As a result, the reconstruction for the eastern Amazon basin displays wetter conditions, because this is the condition recorded by the majority of the proxy records. While the PaleoDA methodology aims to compute the best climate field estimate from all observations, this example demonstrates that the reconstruction may not always align well with individual observations. This spatial smoothing effect due to the model covari-
580 ances has been noted in PaleoDA literature before, e.g., Sanchez et al. (2021), who focused on ENSO reconstructed from coral records during the 19th century, or Erb et al. (2022) who reconstructed the entire Holocene (see the outstanding proxy record anomalies in their Figure 10). In statistical terms, PaleoDA with the EnKF may cause a loss of spatial degrees of freedom in the reconstruction, which can be expressed in terms of the explained variance of the leading modes obtained via a Principal Component Analysis (Bretherton et al., 1999). We are not aware of studies investigating climate field reconstructions under the
585 aspect of spatial degrees of freedom, and doing so would be out of scope for this study. However, we note that when investigating spatial temperature correlations of CE reconstructions, Bakker et al. (2022) found larger inter-continental correlations for a PaleoDA reconstruction product compared to other methods (see their Figure 5). Although our reconstruction product is provided at a spatial resolution of 1.875° x 1.875°, it is more likely to reliably represent spatially extensive regions rather than single grid cells. This aspect is further emphasized by the fact that the climate model simulation data was up-sampled to the
590 resolution of the model with the highest spatial resolution.

Despite using five different isotope-enabled climate model simulations to mitigate the effect of single model biases, an ensemble of five models still represents a small ensemble of opportunity. Further, water isotopes have not been included in climate model intercomparison projects, and the number of publicly available simulations is limited to the five models we have employed. The reconstruction would importantly benefit from more isotope-enabled simulations with a variety of models and more up-to-date forcing, such as volcanic forcing (e.g Sigl et al., 2015). Future PaleoDA reconstructions will also profit from explicitly studying the differences in spatial covariances simulated by the models to potentially discard overly or undersensitive models (e.g., in the covariance relationship of $\delta^{18}O$ values and precipitation changes). Multi-model reconstructions should further account for similarities between models in the form of weighted ensembles (Eyring et al., 2019). Alternatively, perturbed physics ensembles of isotope-enabled simulations for a single model would allow for larger ensembles and a transient offline PaleoDA approach as used by Franke et al. (2017) and Valler et al. (2020). The high computational cost of including water isotopes in the simulations currently restrains this type of experiment.

PaleoDA reconstructions going back deeper in time have also employed prior ensembles that are moving with time to account for changing boundary conditions and, thus, the non-stationarity of simulated covariances (Osman et al., 2021; Erb et al., 2022). However, the time scales on which covariance patterns of specific hydroclimate variables in the climate system change have not been studied formally yet.

6.3 Multi-decadal hydroclimate variability in the reconstruction

We also studied the reconstructed hydroclimate variability to assess the impact of different proxy archives, particularly speleothems. The power spectral distributions of the reconstructed SASM precipitation strength underscore that the use of different climate archives yields distinct hydroclimate variability patterns. Remarkably, the inclusion of speleothems lead to substantial variability increase on multi-decadal to centennial time scales, contributing to a potentially more realistic reconstruction of the South American hydroclimate.

The signficant multi-centennial variability of the SASM (Fig. 6) is comparable, albeit less pronounced and persistent, to findings in individual speleothem records (Novello et al., 2012; Apaéstegui et al., 2014; Novello et al., 2016; Deininger et al., 2019), where this variability was attributed to solar cycles of 83 and 208 years. However, it is essential to consider that the reconstructed 2000-year time series is probably too short to definitively establish causal relationships for multi-centennial variability. Previous research found only small attributions of solar forcing over the last millennium (Schurer et al., 2013). Future PaleoDA reconstructions using speleothem data may focus on longer reconstruction periods to more thoroughly investigate links to solar forcing. The resemblance between the reconstructed hydroclimate variability in our study and the estimates from single proxy record studies is expected, given that we use data from these studies as input. However, PaleoDA enables us to underscore the connection between the isotopic composition of precipitation and precipitation amount. Moreover, spectral analyses derived from proxy record compilations generally yield more reliable estimates of hydroclimate variability.

Our study did not explicitly aim to compare hydroclimate variability in the reconstruction with that of climate model simulations. However, initial analyses reveal a more pronounced multi-decadal to centennial hydroclimate variability in the reconstruction, corroborating previous model-data comparisons for speleothems and isotope-enabled climate models. For tropical

625 South America, (Orrison et al., 2022) demonstrated that the GISS and iCESM last millennium simulations underestimate centennial monsoon intensity changes in the isotopic composition of precipitation. On a global scale, (Bühler et al., 2020) found an underestimation of multi-decadal to centennial variability, using climate simulations also included in our study. A similar underestimation of multi-decadal to centennial variability was previously found for precipitation in the CMIP5 Last Millennium ensemble both for tropical South America (Parsons et al., 2018) and globally (Ault et al., 2012; Parsons et al., 2017),

630 where the spectra were shown to resemble that of white noise. Additionally, for temperature, it is now established that while climate models generally capture the climate variability of global mean temperature, they underestimate regional temperature variability (Laepple et al., 2023b). Our PaleoDA reconstruction, thus, represents a compromise between climate models and climate proxy records, potentially providing a more realistic representation of hydroclimate variability scaling than models alone. We emphasize that the reconstruction of multi-decadal to centennial variability would not have been feasible without

635 the multi-timescale PaleoDA approach, enabling the inclusion of speleothems primarily for technical reasons. It remains to be determined if the use of multi-year covariances, instead of annual ones, in the PaleoDA algorithm also contributed to this, a matter beyond the scope of this publication but suggested by pseudo-proxy experiments (Steiger and Hakim, 2016; Choblet et al., 2023).

In principle, our reconstruction could be employed to investigate interannual variations in SASM strength, for which ENSO is

640 considered a driver (Garreaud et al., 2009). However, we only employed the key archive for SASM variability, the speleothems, at a decadal resolution, even though many of the records technically have a finer resolution. The conservative approach of using decadal time scales for speleothems was adopted to avoid additional complexity arising from dating uncertainty, sampling from age-model ensembles during the reconstruction and taking into account the transit time of cave seepage water. Developing a scheme that considers all these factors would enable to study the influence of ENSO on SASM variability. Employing

645 speleothems at higher resolutions might also improve validation results against 20th-century instrumental precipitation in the region.

6.4 Future developments

To enhance the PaleoDA reconstruction, exploring more elaborate PSMs could be beneficial to perform absolute value reconstructions instead of anomaly reconstructions. In previous work leading up to this study, the speleothem PSM proposed by Dee

650 et al. (2015) was tested, but did not reduce offsets between models proxy records. This can result from either model-biases, from PSMs that do not incorporate processes known to a local cave expert, or from lack of physical understanding of the records. Therefore, we compared simulation and proxy record anomalies by taking known seasonality into account or via a linear regression for tree and coral time series. For speleothems, including information from local cave monitoring studies (e.g. Moquet et al., 2016; Sekhon et al., 2021; Jiménez-Iñiguez et al., 2022), could provide a better understanding of the proxy record

655 and help recognize model biases in simulated $\delta^{18}O$ of precipitation values as well as improve PSMs. However, this usually requires more metadata of individual cave systems, which is not always available and may reduce the selection of usable proxy records.

When employing more elaborate PSMs in PaleoDA, it is essential to test their effect on the covariance patterns as nonlinear mathematical operations can impact covariances unexpectedly. Applying PSMs of higher complexity to instrumental data could also improve the assessment of proxy error and SNR. Although we consider the employed SNR of 0.5 ratio reasonable, it remains a broad assumption due to the lack of sufficiently long instrumental data at the cave locations. Previous PaleoDA reconstructions without clear proxy record error have used a post-hoc adjustment of the error variance (Tierney et al., 2020; Osman et al., 2021). However, we refrain from doing so here, as the tuned errors might be confounded by model biases in the covariances and the proxy record error should represent a real physical and statistical property rather than a tunable hyperparameter. An alternative reconstruction setting proxy record variance equal to the prior record variance yielded similar climate fields with more pronounced magnitudes in hydroclimatic changes (AF D2). Due to the similarity, we have not investigated these reconstructions further, but emphasize, that in the light of the unclear SNR of speleothems and other proxy records, an equal prior/proxy weighting approach would be equally legitimate.

7 Conclusion

This study presents the first South American climate field reconstruction for the entire CE and the entire continent. By incorporating speleothems and other non-annually resolved climate archives through a multi-timescale Data Assimilation approach, we have improved spatial proxy record coverage for South America compared to previous global reconstructions and eliminated the need for uncertain calibration of low-resolution isotopic records to temperature and precipitation. Our primary focus was centered on centennial climate changes, with particular attention to the intensity of the SASM. The reconstruction reveals compelling evidence of a strengthened monsoon during the LIA, contrasting with a weaker SASM before, in particular during the early phase of the MCA. We also found a strengthening during the first centuries of the CE, which remains more elusive due to the more limited number of proxy records. In our reconstruction, speleothems played a vital role in capturing centennial variability.

While this study showcases the potential of the multi-timescale PaleoDA reconstruction approach including speleothems, we acknowledge certain limitations that warrant further investigation. Uncertainties in proxy record errors, spatial smoothing of the reconstruction, and the necessity for a larger ensemble of isotope-enabled climate model simulations with diverse models are important areas for future research. Particular emphasis must be placed on improving the validation of multi-time scale PaleoDA reconstructions based on low-resolution proxy records such as speleothems, as this proves to be particularly challenging due to lack of instrumental data. Our work relies on the assumption that speleothem δ^{18}O values indicate large-scale precipitation changes. This assumption will benefit from further validation, particularly through analysis of speleothem records that reliably capture SASM fluctuations at sub-decadal timescales. The establishment of validation protocols will further help in better assessing the reconstruction skill of multi-time scale PaleoDA reconstructions. Additionally, exploring differences in simulated covariance patterns, fundamental to the PaleoDA EnKF reconstruction algorithm, holds promise for refining and enhancing this methodological approach. We make our reconstructed datasets publicly available, providing a foundation for future climatological data analysis including comparisons to proxy records, other reconstructions, and climate simulations.

Furthermore, by publishing the code for the multi-timescale PaleoDA algorithm alongside this study, we encourage and enable the application of the multi-timescale PaleoDA method to proxy records of different temporal resolutions. This concept has great potential for global climate field reconstructions, particularly for the CE and older time periods, where speleothems and other non-annually and irregularly resolved proxy records serve as essential indicators of past hydroclimate changes.

Code and data availability. Code to reproduce reconstructions, figures and data preprocessing are available on GitHub https://github.com/ mchoblet/paleoda_sa. The reconstructed climate fields are available via a Zenodo repository https://zenodo.org/records/10622264. We recommend using the multi-model ensemble mean of the reconstructions. The input data for running the reconstruction is accessible via a second Zenodo repository https://zenodo.org/records/10370000. We use the model data originally available at https://zenodo.org/records/7516327 (Bühler et al., 2022).

The SISAL (Speleothem Isotopes Synthesis and AnaLysis Working Group) version 3 database (SISALv3) is publicly available at https: //doi.org/10.5287/ora-mzy8pozvk (Kaushal et al., 2023). The PAGES2k Database (Emile-Geay et al., 2017) is available at https://lipdverse. org/project/pages2k/. The Iso2K Database (Konecky et al., 2020) is available at https://lipdverse.org/project/iso2k/. The South American Drought Atlas Database is available at https://www.cr2.cl/datos-dendro-sada/. References for the individual records are listed in Appendix A1.

The PaleoDA code and the figures were created using the Python programming language (Van Rossum and De Boer, 1991), version 3.10 and with a collection of open-source packages, notably Xarray (Hoyer and Hamman, 2017), Numpy (Harris et al., 2020a), Matplotlib (Hunter, 2007), Cartopy (Met Office, 2010 - 2015), Pyleoclim (Khider et al., 2022), Scipy (Virtanen et al., 2020), Pandas (Wes McKinney, 2010) and Numba (Lam et al., 2015).

Video supplement. The reconstructed climate fields are also provided for the *all proxy records* reconstruction in animated form for

1. Temperature, Precipitation, SPEI and δ^{18}O climate fields: https://av.tib.eu/media/66877 (DOI: 10.5446/66877).

2. Precipitation reconstruction and monsoon curve side by side, comparison to the reconstruction by Neukom et al. (2019) https://av.tib. eu/media/66879 (DOI: 10.5446/66879).

3. Precipitation reconstruction and monsoon curve side by side, overlaying of the speleothem δ^{18}O anomalies, comparison to the reconstruction by Neukom et al. (2019) https://av.tib.eu/media/66880 (DOI: 10.5446/66880).

Author contributions. MC, JB, VN, NS and KR designed this study. MC developed the PaleoDA code and produced the reconstructions. MC and JB wrote the paper and MC created the figures. VN, NS and KR contributed with data interpretations and to the revisions of the manuscript. All authors approved of the final version of the paper.

Competing interests. The authors declare that they have no conflict of interest.

Acknowledgements. We thank Raphael Neukom and one anonymous referee for insightful comments and helpful suggestions, which helped in improving the quality of our reconstructions and the manuscript. As this study includes data complied by SISAL (Speleothem Isotopes Synthesis and Analysis), we thank the Pages2k and the Iso2k network, working groups of the Past Global Changes (PAGES) project. We thank all initial authors that provided model simulation data, proxy record data and those researchers who compiled the proxy record databases. We thank Mariano Morales from CONICET, Argentina for sharing tree ring data from the South American Drought Atlas and further tree ring

collections and Michael Erb and Matt Osman for fruitful discussions about PaleoDA. Nils Weitzel, Beatrice Ellerhoff and Markus Maisch are acknowledged for helpful advice and comments during the elaboration of this project.

Financial support. This research has been supported by the Deutsche Forschungsgemeinschaft (grant nos. 316076679, 395588486, and 442926051) and the Bundesministerium für Bildung und Forschung through the PalMod project (grant no. 01LP1926C). NS is supported by the Israel Science Foundation (grant no. 2654/20). We acknowledge support from the Open Access Publication Fund of the University of Tübingen.

References

Aceituno, P., del Rosario Prieto, M., Solari, M. E., Martínez, A., Poveda, G., and Falvey, M.: The 1877–1878 El Niño episode: associated impacts in South America, Climatic Change, 92, 389–416, https://doi.org/10.1007/s10584-008-9470-5, 2008.

Adams, J.: climate indices, an open source Python library providing reference implementations of commonly used climate indices, https://github.com/monocongo/climate_indices, 2017.

Anchukaitis, K. J. and Smerdon, J. E.: Progress and Uncertainties in Global and Hemispheric Temperature Reconstructions of the Common Era, Quaternary Science Reviews, 286, 107 537, https://doi.org/10.1016/j.quascirev.2022.107537, 2022.

Annan, J. D., Hargreaves, J. C., and Mauritsen, T.: A New Global Surface Temperature Reconstruction for the Last Glacial Maximum, Climate of the Past, 18, 1883–1896, https://doi.org/10.5194/cp-18-1883-2022, 2022.

Apaéstegui, J., Cruz, F. W., Sifeddine, A., Vuille, M., Espinoza, J. C., Guyot, J. L., Khodri, M., Strikis, N., Santos, R. V., Cheng, H., Edwards, L., Carvalho, E., and Santini, W.: Hydroclimate Variability of the Northwestern Amazon Basin near the Andean Foothills of Peru Related to the South American Monsoon System during the Last 1600 Years, Climate of the Past, 10, 1967–1981, https://doi.org/10.5194/cp-10-1967-2014, 2014.

Apaéstegui, J., Cruz, F. W., Vuille, M., Fohlmeister, J., Espinoza, J. C., Sifeddine, A., Strikis, N., Guyot, J. L., Ventura, R., Cheng, H., and Edwards, R. L.: Precipitation Changes over the Eastern Bolivian Andes Inferred from Speleothem (δ18O) Records for the Last 1400 Years, Earth and Planetary Science Letters, 494, 124–134, https://doi.org/10.1016/j.epsl.2018.04.048, 2018.

Atsawawaranunt, K., Comas-Bru, L., Amirnezhad Mozhdehi, S., Deininger, M., Harrison, S. P., Baker, A., Boyd, M., Kaushal, N., Ahmad, S. M., Ait Brahim, Y., Arienzo, M., Bajo, P., Braun, K., Burstyn, Y., Chawchai, S., Duan, W., Hatvani, I. G., Hu, J., Kern, Z., Labuhn, I., Lachniet, M., Lechleitner, F. A., Lorrey, A., Pérez-Mejías, C., Pickering, R., Scroxton, N., and SISAL Working Group Members: The SISAL Database: A Global Resource to Document Oxygen and Carbon Isotope Records from Speleothems, Earth System Science Data, 10, 1687–1713, https://doi.org/10.5194/essd-10-1687-2018, 2018.

Ault, T. R., Cole, J. E., and St. George, S.: The amplitude of decadal to multidecadal variability in precipitation simulated by state-of-the-art climate models, Geophysical Research Letters, 39, https://doi.org/10.1029/2012gl053424, 2012.

Azevedo, V., Stríkis, N. M., Santos, R. A., de Souza, J. G., Ampuero, A., Cruz, F. W., de Oliveira, P., Iriarte, J., Stumpf, C. F., Vuille, M., Mendes, V. R., Cheng, H., and Edwards, R. L.: Medieval Climate Variability in the Eastern Amazon-Cerrado Regions and Its Archeological Implications, Scientific Reports, 9, 20 306, https://doi.org/10.1038/s41598-019-56852-7, 2019.

Bakker, P., Goosse, H., and Roche, D. M.: Internal climate variability and spatial temperature correlations during the past 2000 years, Climate of the Past, 18, 2523–2544, 2022.

Beguería, S., Vicente-Serrano, S. M., Reig, F., and Latorre, B.: Standardized Precipitation Evapotranspiration Index (SPEI) Revisited: Parameter Fitting, Evapotranspiration Models, Tools, Datasets and Drought Monitoring, International Journal of Climatology, 34, 3001–3023, https://doi.org/10.1002/joc.3887, 2014.

Bernal, J., Cruz, F. W., Stríkis, N. M., Wang, X., Deininger, M., Catunda, M. C. A., Ortega-Obregón, C., Cheng, H., Edwards, R. L., and Auler, A. S.: High-resolution Holocene South American monsoon history recorded by a speleothem from Botuverá Cave, Brazil, Earth and Planetary Science Letters, 450, 186–196, https://doi.org/10.1016/j.epsl.2016.06.008, 2016.

Bhend, J., Franke, J., Folini, D., Wild, M., and Brönnimann, S.: An Ensemble-Based Approach to Climate Reconstructions, Climate of the Past, 8, 963–976, https://doi.org/10.5194/cp-8-963-2012, 2012.

Bird, B. W., Abbott, M. B., Rodbell, D. T., and Vuille, M.: Holocene Tropical South American Hydroclimate Revealed from a Decadally Resolved Lake Sediment $\delta 18O$ Record, Earth and Planetary Science Letters, 310, 192–202, https://doi.org/10.1016/j.epsl.2011.08.040, 2011.

Bishop, C. H., Etherton, B. J., and Majumdar, S. J.: Adaptive Sampling with the Ensemble Transform Kalman Filter. Part I: Theoretical Aspects, Monthly Weather Review, 129, 420–436, https://doi.org/10.1175/1520-0493(2001)129<0420:ASWTET>2.0.CO;2, 2001.

Boucher, É., Guiot, J., and Chapron, E.: A Millennial Multi-Proxy Reconstruction of Summer PDSI for Southern South America, Climate of the Past, 7, 957–974, https://doi.org/10.5194/cp-7-957-2011, 2011.

Bradley, R.: Paleoclimatology. Reconstructing Climates of the Quaternary., Elsevier, 2015.

Brady, E., Stevenson, S., Bailey, D., Liu, Z., Noone, D., Nusbaumer, J., Otto-Bliesner, B. L., Tabor, C., Tomas, R., Wong, T., Zhang, J., and Zhu, J.: The Connected Isotopic Water Cycle in the Community Earth System Model Version 1, Journal of Advances in Modeling Earth Systems, 11, 2547–2566, https://doi.org/10.1029/2019MS001663, 2019.

Bretherton, C. S., Widmann, M., Dymnikov, V. P., Wallace, J. M., and Bladé, I.: The Effective Number of Spatial Degrees of Freedom of a Time-Varying Field, Journal of Climate, 12, 1990–2009, https://doi.org/10.1175/1520-0442(1999)012<1990:TENOSD>2.0.CO;2, 1999.

Bühler, J. C., Roesch, C., Kirschner, M., Sime, L., Holloway, M. D., and Rehfeld, K.: Comparison of the Oxygen Isotope Signatures in Speleothem Records and iHadCM3 Model Simulations for the Last Millennium, Preprint, Climate Modelling/Terrestrial Archives/Centennial-Decadal, https://doi.org/10.5194/cp-2020-121, 2020.

Bühler, J. C., Roesch, C., Kirschner, M., Sime, L., Holloway, M. D., and Rehfeld, K.: Comparison of the Oxygen Isotope Signatures in Speleothem Records and iHadCM3 Model Simulations for the Last Millennium, Climate of the Past, 17, 985–1004, https://doi.org/10.5194/cp-17-985-2021, 2021.

Bühler, J. C., Axelsson, J., Lechleitner, F. A., Fohlmeister, J., LeGrande, A. N., Midhun, M., Sjolte, J., Werner, M., Yoshimura, K., and Rehfeld, K.: Investigating Stable Oxygen and Carbon Isotopic Variability in Speleothem Records over the Last Millennium Using Multiple Isotope-Enabled Climate Models, Climate of the Past, 18, 1625–1654, https://doi.org/10.5194/cp-18-1625-2022, 2022.

Bühler, J. C., Axelsson, J., Rehfeld, K., LeGrande, A. N., Midhun, M., Sjolte, J., Werner, M., and Yoshimura, K.: Monthly climate variables of isotope-enabled climate model simulations over the last millennium (850-1849CE), https://doi.org/10.5281/ZENODO.6610684, 2022.

Campos, J. L. P. S., Cruz, F. W., Ambrizzi, T., Deininger, M., Vuille, M., Novello, V. F., and Strikis, N. M.: Coherent South American Monsoon Variability During the Last Millennium Revealed Through High-Resolution Proxy Records, Geophysical Research Letters, 46, 8261–8270, https://doi.org/10.1029/2019GL082513, 2019.

Campos, M. C., Chiessi, C. M., Novello, V. F., Crivellari, S., Campos, J. L. P. S., Albuquerque, A. L. S., Venancio, I. M., Santos, T. P., Melo, D. B., Cruz, F. W., Sawakuchi, A. O., and Mendes, V. R.: South American Precipitation Dipole Forced by Interhemispheric Temperature Gradient, Scientific Reports, 12, 10 527, https://doi.org/10.1038/s41598-022-14495-1, 2022.

Carvalho, L. M. V., Jones, C., and Liebmann, B.: The South Atlantic Convergence Zone: Intensity, Form, Persistence, and Relationships with Intraseasonal to Interannual Activity and Extreme Rainfall, Journal of Climate, 17, 88–108, https://doi.org/10.1175/1520-0442(2004)017<0088:tsaczi>2.0.co;2, 2004.

Choblet, M. A., Bühler, J. C., Steiger, N. J., Novello, V. F., and Rehfeld, K.: Reconstructing climate fields with terrestrial climate archives, isotope-enabled GCMs and Data Assimilation, Copernicus GmbH, https://doi.org/10.5194/egusphere-egu23-2600, 2023.

Colose, C. M., LeGrande, A. N., and Vuille, M.: Hemispherically Asymmetric Volcanic Forcing of Tropical Hydroclimate during the Last Millennium, Earth System Dynamics, 7, 681–696, https://doi.org/10.5194/esd-7-681-2016, 2016a.

Colose, C. M., LeGrande, A. N., and Vuille, M.: The Influence of Volcanic Eruptions on the Climate of Tropical South America during the Last Millennium in an Isotope-Enabled General Circulation Model, Climate of the Past, 12, 961–979, https://doi.org/10.5194/cp-12-961-2016, 2016b.

Comas-Bru, L., Rehfeld, K., Roesch, C., Amirnezhad-Mozhdehi, S., Harrison, S. P., Atsawawaranunt, K., Ahmad, S. M., Brahim, Y. A., Baker, A., Bosomworth, M., Breitenbach, S. F. M., Burstyn, Y., Columbu, A., Deininger, M., Demény, A., Dixon, B., Fohlmeister, J., Hatvani, I. G., Hu, J., Kaushal, N., Kern, Z., Labuhn, I., Lechleitner, F. A., Lorrey, A., Martrat, B., Novello, V. F., Oster, J., Pérez-Mejías, C., Scholz, D., Scroxton, N., Sinha, N., Ward, B. M., Warken, S., Zhang, H., and SISAL Working Group members: SISALv2: A Comprehensive Speleothem Isotope Database with Multiple Age–Depth Models, Earth System Science Data, 12, 2579–2606, https://doi.org/10.5194/essd-12-2579-2020, 2020.

Comboul, M., Emile-Geay, J., Hakim, G. J., and Evans, M. N.: Paleoclimate Sampling as a Sensor Placement Problem, Journal of Climate, 28, 7717–7740, https://doi.org/10.1175/JCLI-D-14-00802.1, 2015.

Cook, E. R., Meko, D. M., Stahle, D. W., and Cleaveland, M. K.: Drought Reconstructions for the Continental United States*, Journal of Climate, 12, 1145–1162, https://doi.org/10.1175/1520-0442(1999)012<1145:drftcu>2.0.co;2, 1999.

Craig, H.: Isotopic variations in meteoric waters, Science, 133, 1702–1703, 1961.

Cruz, F. W., Vuille, M., Burns, S. J., Wang, X., Cheng, H., Werner, M., Edwards, R. L., Karmann, I., Auler, A. S., and Nguyen, H.: Orbitally driven east–west antiphasing of South American precipitation, Nature Geoscience, 2, 210–214, https://doi.org/10.1038/ngeo444, 2009.

Dansgaard, W.: Stable Isotopes in Precipitation, Tellus, 16, 436–468, https://doi.org/10.1111/j.2153-3490.1964.tb00181.x, 1964.

de Souza, J. G., Robinson, M., Maezumi, S. Y., Capriles, J., Hoggarth, J. A., Lombardo, U., Novello, V. F., Apaéstegui, J., Whitney, B., Urrego, D., Alves, D. T., Rostain, S., Power, M. J., Mayle, F. E., da Cruz, F. W., Hooghiemstra, H., and Iriarte, J.: Climate Change and Cultural Resilience in Late Pre-Columbian Amazonia, Nature Ecology & Evolution, 3, 1007–1017, https://doi.org/10.1038/s41559-019-0924-0, 2019.

Dee, S., Emile-Geay, J., Evans, M. N., Allam, A., Steig, E. J., and Thompson, D.: PRYSM: An Open-Source Framework for PRoxY System Modeling, with Applications to Oxygen-Isotope Systems, Journal of Advances in Modeling Earth Systems, 7, 1220–1247, https://doi.org/10.1002/2015MS000447, 2015.

Dee, S. G., Steiger, N. J., Emile-Geay, J., and Hakim, G. J.: On the utility of proxy system models for estimating climate states over the common era, Journal of Advances in Modeling Earth Systems, 8, 1164–1179, https://doi.org/10.1002/2016ms000677, 2016.

Deininger, M., Ward, B. M., Novello, V. F., and Cruz, F. W.: Late Quaternary Variations in the South American Monsoon System as Inferred by Speleothems—New Perspectives Using the SISAL Database, Quaternary, 2, 6, https://doi.org/10.3390/quat2010006, 2019.

Dirren, S. and Hakim, G. J.: Toward the assimilation of time-averaged observations, Geophysical research letters, 32, 2005.

Emile-Geay, J., McKay, N. P., Kaufman, D. S., von Gunten, L., Wang, J., Anchukaitis, K. J., Abram, N. J., Addison, J. A., Curran, M. A., Evans, M. N., Henley, B. J., Hao, Z., Martrat, B., McGregor, H. V., Neukom, R., Pederson, G. T., Stenni, B., Thirumalai, K., Werner, J. P., Xu, C., Divine, D. V., Dixon, B. C., Gergis, J., Mundo, I. A., Nakatsuka, T., Phipps, S. J., Routson, C. C., Steig, E. J., Tierney, J. E., Tyler, J. J., Allen, K. J., Bertler, N. A., Björklund, J., Chase, B. M., Chen, M.-T., Cook, E., de Jong, R., DeLong, K. L., Dixon, D. A., Ekaykin, A. A., Ersek, V., Filipsson, H. L., Francus, P., Freund, M. B., Frezzotti, M., Gaire, N. P., Gajewski, K., Ge, Q., Goosse, H., Gornostaeva, A., Grosjean, M., Horiuchi, K., Hormes, A., Husum, K., Isaksson, E., Kandasamy, S., Kawamura, K., Kilbourne, K. H., Koç, N., Leduc, G., Linderholm, H. W., Lorrey, A. M., Mikhalenko, V., Mortyn, P. G., Motoyama, H., Moy, A. D., Mulvaney, R., Munz, P. M., Nash, D. J., Oerter, H., Opel, T., Orsi, A. J., Ovchinnikov, D. V., Porter, T. J., Roop, H. A., Saenger, C., Sano, M., Sauchyn, D., Saunders, K. M., Seidenkrantz, M.-S., Severi, M., Shao, X., Sicre, M.-A., Sigl, M., Sinclair, K., St. George, S., St. Jacques, J.-M., Thamban, M.,

Kuwar Thapa, U., Thomas, E. R., Turney, C., Uemura, R., Viau, A. E., Vladimirova, D. O., Wahl, E. R., White, J. W., Yu, Z., Zinke, J., and PAGES2k Consortium: A Global Multiproxy Database for Temperature Reconstructions of the Common Era, Scientific Data, 4, 170 088, https://doi.org/10.1038/sdata.2017.88, 2017.

Erb, M. P., McKay, N. P., Steiger, N., Dee, S., Hancock, C., Ivanovic, R. F., Gregoire, L. J., and Valdes, P.: Reconstructing Holocene Temperatures in Time and Space Using Paleoclimate Data Assimilation, Climate of the Past, 18, 2599–2629, https://doi.org/10.5194/cp-18-2599-2022, 2022.

Evans, M. N., Tolwinski-Ward, S. E., Thompson, D. M., and Anchukaitis, K. J.: Applications of Proxy System Modeling in High Resolution Paleoclimatology, Quaternary Science Reviews, 76, 16–28, https://doi.org/10.1016/j.quascirev.2013.05.024, 2013.

Evensen, G.: Sequential Data Assimilation with a Nonlinear Quasi-Geostrophic Model Using Monte Carlo Methods to Forecast Error Statistics, Journal of Geophysical Research: Oceans, 99, 10 143–10 162, https://doi.org/10.1029/94JC00572, 1994.

Evensen, G.: The Ensemble Kalman Filter: Theoretical Formulation and Practical Implementation, Ocean Dynamics, 53, 343–367, https://doi.org/10.1007/s10236-003-0036-9, 2003.

Evensen, G., Vossepoel, F. C., and van Leeuwen, P. J.: Data Assimilation Fundamentals: A Unified Formulation of the State and Parameter Estimation Problem, Springer Textbooks in Earth Sciences, Geography and Environment, Springer International Publishing, Cham, https://doi.org/10.1007/978-3-030-96709-3, 2022.

Eyring, V., Cox, P. M., Flato, G. M., Gleckler, P. J., Abramowitz, G., Caldwell, P., Collins, W. D., Gier, B. K., Hall, A. D., Hoffman, F. M., et al.: Taking climate model evaluation to the next level, Nature Climate Change, 9, 102–110, 2019.

Franke, J., Brönnimann, S., Bhend, J., and Brugnara, Y.: A Monthly Global Paleo-Reanalysis of the Atmosphere from 1600 to 2005 for Studying Past Climatic Variations, Scientific Data, 4, 170 076, https://doi.org/10.1038/sdata.2017.76, 2017.

Garreaud, R. D., Vuille, M., Compagnucci, R., and Marengo, J.: Present-Day South American Climate, Palaeogeography, Palaeoclimatology, Palaeoecology, 281, 180–195, https://doi.org/10.1016/j.palaeo.2007.10.032, 2009.

Garreaud, R. D., Boisier, J. P., Rondanelli, R., Montecinos, A., Sepúlveda, H. H., and Veloso-Aguila, D.: The Central Chile Mega Drought (2010–2018): A climate dynamics perspective, International Journal of Climatology, 40, 421–439, https://doi.org/10.1002/joc.6219, 2019.

Gioda, A. and Prieto, M. d. R.: Histoire des sécheresses andines ; Potosi, El Niño et le Petit âge glaciaire, La Météorologie, 1999, 33–42, https://doi.org/10.4267/2042/47082, 1999.

Hakim, G. J., Emile-Geay, J., Steig, E. J., Noone, D., Anderson, D. M., Tardif, R., Steiger, N., and Perkins, W. A.: The Last Millennium Climate Reanalysis Project: Framework and First Results, Journal of Geophysical Research: Atmospheres, 121, 6745–6764, https://doi.org/10.1002/2016JD024751, 2016.

Harris, C. R., Millman, K. J., van der Walt, S. J., Gommers, R., Virtanen, P., Cournapeau, D., Wieser, E., Taylor, J., Berg, S., Smith, N. J., Kern, R., Picus, M., Hoyer, S., van Kerkwijk, M. H., Brett, M., Haldane, A., del Río, J. F., Wiebe, M., Peterson, P., Gérard-Marchant, P., Sheppard, K., Reddy, T., Weckesser, W., Abbasi, H., Gohlke, C., and Oliphant, T. E.: Array programming with NumPy, Nature, 585, 357–362, https://doi.org/10.1038/s41586-020-2649-2, 2020a.

Harris, I., Osborn, T. J., Jones, P., and Lister, D.: Version 4 of the CRU TS monthly high-resolution gridded multivariate climate dataset, Scientific Data, 7, https://doi.org/10.1038/s41597-020-0453-3, 2020b.

Hoyer, S. and Hamman, J.: xarray: N-D labeled arrays and datasets in Python, J. Open Res. Software, 2017.

Hunter, J. D.: Matplotlib: A 2D graphics environment, Computing in Science & Engineering, 9, 90–95, https://doi.org/10.1109/MCSE.2007.55, 2007.

Huntley, H. S. and Hakim, G. J.: Assimilation of Time-Averaged Observations in a Quasi-Geostrophic Atmospheric Jet Model, Climate Dynamics, 35, 995–1009, https://doi.org/10.1007/s00382-009-0714-5, 2010.

880 Jiménez-Iñiguez, A., Ampuero, A., Valencia, B. G., Mayta, V. C., Cruz, F. W., Vuille, M., Novello, V. F., Misailidis Stríkis, N., Aranda, N., and Conicelli, B.: Stable isotope variability of precipitation and cave drip-water at Jumandy cave, western Amazon River basin (Ecuador), J. Hydrol. (Amst.), 610, 127 848, 2022.

Jiménez-Iñiguez, A., Ampuero, A., Valencia, B. G., Mayta, V. C., Cruz, F. W., Vuille, M., Novello, V. F., Stríkis, N. M., Aranda, N., and Conicelli, B.: Stable isotope variability of precipitation and cave drip-water at Jumandy cave, western Amazon River basin (Ecuador),
885 Journal of Hydrology, 610, 127 848, https://doi.org/10.1016/j.jhydrol.2022.127848, 2022.

Jungclaus, J. H., Bard, E., Baroni, M., Braconnot, P., Cao, J., Chini, L. P., Egorova, T., Evans, M., González-Rouco, J. F., Goosse, H., Hurtt, G. C., Joos, F., Kaplan, J. O., Khodri, M., Goldewijk, K. K., Krivova, N., LeGrande, A. N., Lorenz, S. J., Luterbacher, J., Man, W., Maycock, A. C., Meinshausen, M., Moberg, A., Muscheler, R., Nehrbass-Ahles, C., Otto-Bliesner, B. I., Phipps, S. J., Pongratz, J., Rozanov, E., Schmidt, G. A., Schmidt, H., Schmutz, W., Schurer, A., Shapiro, A. I., Sigl, M., Smerdon, J. E., Solanki, S. K., Timmreck,
890 C., Toohey, M., Usoskin, I. G., Wagner, S., Wu, C.-J., Yeo, K. L., Zanchettin, D., Zhang, Q., and Zorita, E.: The PMIP4 contribution to CMIP6–Part 3: The last millennium, scientific objective, and experimental design for the PMIP4 past1000 simulations, Geoscientific Model Development, 10, 4005–4033, https://doi.org/10.5194/gmd-10-4005-2017, 2017.

Kaushal, N., Lechleitner, F. A., Wilhelm, M., Bühler, J. C., Braun, K., Brahim, Y. A., Azennoud, K., Baker, A., Burstyn, Y., Comas-Bru, L., Goldsmith, Y., Harrison, S. P., Hatvani, I. G., Rehfeld, K., Ritzau, M., Skiba, V., Stoll, H. M., Szűcs, J. G., Treble, P. C., Azevedo,
895 V., Baker, J. L., Chawchai, S., Columbu, A., Endres, L., Hu, J., Kern, Z., Kimbrough, A., Koç, K., Markowska, M., Martrat, B., Ahmad, S. M., Nehme, C., Novello, V. F., Pérez-Mejías, C., Ruan, J., Sekhon, N., Sinha, N., Tadros, C. V., Tiger, B. H., Warken, S., Wolf, A., and and, H. Z.: SISALv3: A global speleothem stable isotope and trace element database, https://doi.org/10.5194/essd-2023-364, 2023.

Khider, D., Emile-Geay, J., Zhu, F., James, A., Landers, J., Ratnakar, V., and Gil, Y.: Pyleoclim: Paleoclimate Timeseries Analysis and Visualization With Python, Paleoceanography and Paleoclimatology, 37, e2022PA004 509, https://doi.org/10.1029/2022PA004509, 2022.

900 King, J., Anchukaitis, K. J., Allen, K., Vance, T., and Hessl, A.: Trends and Variability in the Southern Annular Mode over the Common Era, Nature Communications, 14, 2324, https://doi.org/10.1038/s41467-023-37643-1, 2023.

King, J. M., Anchukaitis, K. J., Tierney, J. E., Hakim, G. J., Emile-Geay, J., Zhu, F., and Wilson, R.: A Data Assimilation Approach to Last Millennium Temperature Field Reconstruction Using a Limited High-Sensitivity Proxy Network, Journal of Climate, 34, 7091–7111, https://doi.org/10.1175/JCLI-D-20-0661.1, 2021.

905 Konecky, B. L., McKay, N. P., Churakova (Sidorova), O. V., Comas-Bru, L., Dassié, E. P., DeLong, K. L., Falster, G. M., Fischer, M. J., Jones, M. D., Jonkers, L., Kaufman, D. S., Leduc, G., Managave, S. R., Martrat, B., Opel, T., Orsi, A. J., Partin, J. W., Sayani, H. R., Thomas, E. K., Thompson, D. M., Tyler, J. J., Abram, N. J., Atwood, A. R., Cartapanis, O., Conroy, J. L., Curran, M. A., Dee, S. G., Deininger, M., Divine, D. V., Kern, Z., Porter, T. J., Stevenson, S. L., von Gunten, L., and Members, I. P.: The Iso2k Database: A Global Compilation of Paleo-δ^{18}O and δ^2H Records to Aid Understanding of Common Era Climate, Earth System Science Data, 12, 2261–2288,
910 https://doi.org/10.5194/essd-12-2261-2020, 2020.

Laepple, T. and Huybers, P.: Ocean Surface Temperature Variability: Large Model–Data Differences at Decadal and Longer Periods, Proceedings of the National Academy of Sciences, 111, 16 682–16 687, https://doi.org/10.1073/pnas.1412077111, 2014.

Laepple, T., Muench, T., and Dolman, A.: PaleoSpec: Spectral tools for the ECUS group, https://earthsystemdiagnostics.github.io/paleospec/, r package version 0.2.91, 2023a.

915   Laepple, T., Ziegler, E., Weitzel, N., Hébert, R., Ellerhoff, B., Schoch, P., Martrat, B., Bothe, O., Moreno-Chamarro, E., Chevalier, M., Herbert, A., and Rehfeld, K.: Regional but not global temperature variability underestimated by climate models at supradecadal timescales, Nat. Geosci., 16, 958–966, 2023b.

Lam, S. K., Pitrou, A., and Seibert, S.: Numba: A llvm-based python jit compiler, in: Proceedings of the Second Workshop on the LLVM Compiler Infrastructure in HPC, pp. 1–6, 2015.

920   Lewis, S. C. and LeGrande, A. N.: Stability of ENSO and Its Tropical Pacific Teleconnections over the Last Millennium, Climate of the Past, 11, 1347–1360, https://doi.org/10.5194/cp-11-1347-2015, 2015.

Lüning, S., Gałka, M., Bamonte, F. P., Rodríguez, F. G., and Vahrenholt, F.: The medieval climate anomaly in South America, Quaternary International, 508, 70–87, 2019.

Luterbacher, J., Xoplaki, E., Dietrich, D., Rickli, R., Jacobeit, J., Beck, C., Gyalistras, D., Schmutz, C., and Wanner, H.: Reconstruc-
925   tion of Sea Level Pressure Fields over the Eastern North Atlantic and Europe Back to 1500, Climate Dynamics, 18, 545–561, https://doi.org/10.1007/s00382-001-0196-6, 2002.

Luterbacher, J., Neukom, R., González-Rouco, F., Fernandez-Donado, L., Raible, C., and Zorita, E.: Reconstructed and Simulated Medieval Climate Anomaly in Southern South America, PAGES news, 19, 20–21, https://doi.org/10.22498/pages.19.1.20, 2011.

Marengo, J. A., Liebmann, B., Grimm, A. M., Misra, V., Silva Dias, P. L., Cavalcanti, I. F. A., Carvalho, L. M. V., Berbery, E. H., Ambrizzi,
930   T., Vera, C. S., Saulo, A. C., Nogues-Paegle, J., Zipser, E., Seth, A., and Alves, L. M.: Recent developments on the South American monsoon system, International Journal of Climatology, 32, 1–21, https://doi.org/10.1002/joc.2254, 2010.

Met Office: Cartopy: a cartographic python library with a Matplotlib interface, Exeter, Devon, https://scitools.org.uk/cartopy, 2010 - 2015.

Moquet, J. S., Cruz, F. W., Novello, V. F., Stríkis, N. M., Deininger, M., Karmann, I., Santos, R. V., Millo, C., Apaestegui, J., Guyot, J. L., Siffedine, A., Vuille, M., Cheng, H., Edwards, R. L., and Santini, W.: Calibration of Speleothem $\delta18O$ Records against Hydroclimate
935   Instrumental Records in Central Brazil, Global and Planetary Change, 139, 151–164, https://doi.org/10.1016/j.gloplacha.2016.02.001, 2016.

Morales, M. S., Cook, E. R., Barichivich, J., Christie, D. A., Villalba, R., LeQuesne, C., Srur, A. M., Ferrero, M. E., González-Reyes, Á., Couvreux, F., et al.: Six hundred years of South American tree rings reveal an increase in severe hydroclimatic events since mid-20th century, Proceedings of the National Academy of Sciences, 117, 16 816–16 823, 2020.

940   Nash, J. E. and Sutcliffe, J. V.: River Flow Forecasting through Conceptual Models Part I — A Discussion of Principles, Journal of Hydrology, 10, 282–290, https://doi.org/10.1016/0022-1694(70)90255-6, 1970.

Neukom, R. and Gergis, J.: Southern Hemisphere High-Resolution Palaeoclimate Records of the Last 2000 Years, The Holocene, 22, 501–524, https://doi.org/10.1177/0959683611427335, 2012.

Neukom, R., del Rosario Prieto, M., Moyano, R., Luterbacher, J., Pfister, C., Villalba, R., Jones, P. D., and Wanner, H.: An Extended
945   Network of Documentary Data from South America and Its Potential for Quantitative Precipitation Reconstructions Back to the 16th Century, Geophysical Research Letters, 36, L12 703, https://doi.org/10.1029/2009GL038351, 2009.

Neukom, R., Luterbacher, J., Villalba, R., Küttel, M., Frank, D., Jones, P. D., Grosjean, M., Esper, J., Lopez, L., and Wanner, H.: Multi-Centennial Summer and Winter Precipitation Variability in Southern South America, Geophysical Research Letters, 37, https://doi.org/10.1029/2010GL043680, 2010.

950   Neukom, R., Luterbacher, J., Villalba, R., Küttel, M., Frank, D., Jones, P. D., Grosjean, M., Wanner, H., Aravena, J.-C., Black, D. E., et al.: Multiproxy summer and winter surface air temperature field reconstructions for southern South America covering the past centuries, Climate Dynamics, 37, 35–51, 2011.

Neukom, R., Gergis, J., Karoly, D., Wanner, H., Curran, M., Elbert, J., González Rouco, J. F., Linsley, B., Moy, A., Mundo, I., Raible, C., Steig, E., van Ommen, T., Vance, T., Villalba, R., Zinke, J., and Frank, D.: Inter-Hemispheric Temperature Variability over the Last Millennium, Nature Climate Change, 4, https://doi.org/10.1038/nclimate2174, 2014.

Neukom, R., Steiger, N., Gómez-Navarro, J. J., Wang, J., and Werner, J. P.: No Evidence for Globally Coherent Warm and Cold Periods over the Preindustrial Common Era, Nature, 571, 550–554, https://doi.org/10.1038/s41586-019-1401-2, 2019.

Novello, V. F., Cruz, F. W., Karmann, I., Burns, S. J., Stríkis, N. M., Vuille, M., Cheng, H., Lawrence Edwards, R., Santos, R. V., Frigo, E., and Barreto, E. A. S.: Multidecadal Climate Variability in Brazil's Nordeste during the Last 3000 Years Based on Speleothem Isotope Records, Geophysical Research Letters, 39, https://doi.org/10.1029/2012GL053936, 2012.

Novello, V. F., Vuille, M., Cruz, F. W., Stríkis, N. M., de Paula, M. S., Edwards, R. L., Cheng, H., Karmann, I., Jaqueto, P. F., Trindade, R. I. F., Hartmann, G. A., and Moquet, J. S.: Centennial-Scale Solar Forcing of the South American Monsoon System Recorded in Stalagmites, Scientific Reports, 6, 24 762, https://doi.org/10.1038/srep24762, 2016.

Novello, V. F., Cruz, F. W., Moquet, J. S., Vuille, M., de Paula, M. S., Nunes, D., Edwards, R. L., Cheng, H., Karmann, I., Utida, G., Stríkis, N. M., and Campos, J. L. P. S.: Two Millennia of South Atlantic Convergence Zone Variability Reconstructed From Isotopic Proxies, Geophysical Research Letters, 45, 5045–5051, https://doi.org/10.1029/2017GL076838, 2018.

Okazaki, A., Miyoshi, T., Yoshimura, K., Greybush, S. J., and Zhang, F.: Revisiting Online and Offline Data Assimilation Comparison for Paleoclimate Reconstruction: An Idealized OSSE Study, Journal of Geophysical Research: Atmospheres, 126, e2020JD034 214, https://doi.org/10.1029/2020JD034214, 2021.

Oke, P. R., Schiller, A., Griffin, D. A., and Brassington, G. B.: Ensemble Data Assimilation for an Eddy-Resolving Ocean Model of the Australian Region, Quarterly Journal of the Royal Meteorological Society, 131, 3301–3311, https://doi.org/10.1256/qj.05.95, 2005.

Orrison, R., Vuille, M., Smerdon, J. E., Apaéstegui, J., Azevedo, V., Campos, J. L. P. S., Cruz, F. W., Della Libera, M. E., and Stríkis, N. M.: South American Summer Monsoon Variability over the Last Millennium in Paleoclimate Records and Isotope-Enabled Climate Models, Climate of the Past, 18, 2045–2062, https://doi.org/10.5194/cp-18-2045-2022, 2022.

Osman, M. B., Tierney, J. E., Zhu, J., Tardif, R., Hakim, G. J., King, J., and Poulsen, C. J.: Globally Resolved Surface Temperatures since the Last Glacial Maximum, Nature, 599, 239–244, https://doi.org/10.1038/s41586-021-03984-4, 2021.

PAGES 2k Consortium: [SI] Consistent Multidecadal Variability in Global Temperature Reconstructions and Simulations over the Common Era, Nature Geoscience, 12, 643–649, https://doi.org/10.1038/s41561-019-0400-0, 2019.

Parsons, L. A., Loope, G. R., Overpeck, J. T., Ault, T. R., Stouffer, R., and Cole, J. E.: Temperature and Precipitation Variance in CMIP5 Simulations and Paleoclimate Records of the Last Millennium, Journal of Climate, 30, 8885–8912, https://doi.org/10.1175/jcli-d-16-0863.1, 2017.

Parsons, L. A., LeRoy, S., Overpeck, J. T., Bush, M., Cárdenes-Sandí, G., and Saleska, S.: The Threat of Multi-Year Drought in Western Amazonia, Water Resources Research, 54, 5890–5904, https://doi.org/10.1029/2017wr021788, 2018.

Parsons, L. A., Amrhein, D. E., Sanchez, S. C., Tardif, R., Brennan, M. K., and Hakim, G. J.: Do Multi-Model Ensembles Improve Reconstruction Skill in Paleoclimate Data Assimilation?, Earth and Space Science, 8, e2020EA001 467, https://doi.org/10.1029/2020EA001467, 2021.

Pörtner, H.-O., Roberts, D. C., Poloczanska, E. S., Mintenbeck, K., Tignor, M., Alegría, A., Craig, M., Langsdorf, S., Löschke, S., Möller, V., et al.: IPCC, 2022: Summary for policymakers, 2022.

Prieto, M. d. R.: ENSO Signals in South America: Rains and Floods in the Paraná River Region during Colonial Times, Climatic Change, 83, 39–54, https://doi.org/10.1007/s10584-006-9188-1, 2007.

Prieto, M. d. R. and García Herrera, R.: Documentary Sources from South America: Potential for Climate Reconstruction, Palaeogeography, Palaeoclimatology, Palaeoecology, 281, 196–209, https://doi.org/10.1016/j.palaeo.2008.07.026, 2009.

Rohde, R. A. and Hausfather, Z.: The Berkeley Earth Land/Ocean Temperature Record, Earth System Science Data, 12, 3469–3479, https://doi.org/10.5194/essd-12-3469-2020, 2020.

995 Rojas, M., Arias, P. A., Flores-Aqueveque, V., Seth, A., and Vuille, M.: The South American Monsoon Variability over the Last Millennium in Climate Models, Climate of the Past, 12, 1681–1691, https://doi.org/10.5194/cp-12-1681-2016, 2016.

Sanchez, S. C., Hakim, G. J., and Saenger, C. P.: Climate Model Teleconnection Patterns Govern the Niño-3.4 Response to Early Nineteenth-Century Volcanism in Coral-Based Data Assimilation Reconstructions, Journal of Climate, 34, 1863–1880, https://doi.org/10.1175/JCLI-D-20-0549.1, 2021.

1000 Schurer, A. P., Tett, S. F. B., and Hegerl, G. C.: Small influence of solar variability on climate over the past millennium, Nature Geoscience, 7, 104–108, https://doi.org/10.1038/ngeo2040, 2013.

Sekhon, N., Novello, V. F., Cruz, F. W., Wortham, B. E., Ribeiro, T. G., and Breecker, D. O.: Diurnal to seasonal ventilation in Brazilian caves, Global and Planetary Change, 197, 103 378, https://doi.org/10.1016/j.gloplacha.2020.103378, 2021.

Sigl, M., Winstrup, M., McConnell, J. R., Welten, K. C., Plunkett, G., Ludlow, F., Büntgen, U., Caffee, M., Chellman, N., Dahl-Jensen, D.,
1005 et al.: Timing and climate forcing of volcanic eruptions for the past 2,500 years, Nature, 523, 543–549, 2015.

Sjolte, J., Adolphi, F., Vinther, B. M., Muscheler, R., Sturm, C., Werner, M., and Lohmann, G.: Seasonal Reconstructions Coupling Ice Core Data and an Isotope-Enabled Climate Model – Methodological Implications of Seasonality, Climate Modes and Selection of Proxy Data, Climate of the Past, 16, 1737–1758, https://doi.org/10.5194/cp-16-1737-2020, 2020.

Smerdon, J. E.: Climate Models as a Test Bed for Climate Reconstruction Methods: Pseudoproxy Experiments: Pseudoproxy Experiments,
1010 Wiley Interdisciplinary Reviews: Climate Change, 3, 63–77, https://doi.org/10.1002/wcc.149, 2012.

Steiger, N. and Hakim, G.: Multi-Timescale Data Assimilation for Atmosphere–Ocean State Estimates, Climate of the Past, 12, 1375–1388, https://doi.org/10.5194/cp-12-1375-2016, 2016.

Steiger, N. J., Hakim, G. J., Steig, E. J., Battisti, D. S., and Roe, G. H.: Assimilation of Time-Averaged Pseudoproxies for Climate Reconstruction, Journal of Climate, 27, 426–441, https://doi.org/10.1175/JCLI-D-12-00693.1, 2014.

1015 Steiger, N. J., Smerdon, J. E., Cook, E. R., and Cook, B. I.: A Reconstruction of Global Hydroclimate and Dynamical Variables over the Common Era, Scientific Data, 5, 180 086, https://doi.org/10.1038/sdata.2018.86, 2018.

Stevenson, S., Otto-Bliesner, B. L., Brady, E. C., Nusbaumer, J., Tabor, C., Tomas, R., Noone, D. C., and Liu, Z.: Volcanic Eruption Signatures in the Isotope-Enabled Last Millennium Ensemble, Paleoceanography and Paleoclimatology, 34, 1534–1552, https://doi.org/10.1029/2019PA003625, 2019.

1020 Tardif, R., Hakim, G. J., Perkins, W. A., Horlick, K. A., Erb, M. P., Emile-Geay, J., Anderson, D. M., Steig, E. J., and Noone, D.: Last Millennium Reanalysis with an Expanded Proxy Database and Seasonal Proxy Modeling, Climate of the Past, 15, 1251–1273, https://doi.org/10.5194/cp-15-1251-2019, 2019.

Tierney, J. E., Zhu, J., King, J., Malevich, S. B., Hakim, G. J., and Poulsen, C. J.: Glacial Cooling and Climate Sensitivity Revisited, Nature, 584, 569–573, https://doi.org/10.1038/s41586-020-2617-x, 2020.

1025 Tierney, J. E., Zhu, J., Li, M., Ridgwell, A., Hakim, G. J., Poulsen, C. J., Whiteford, R. D. M., Rae, J. W. B., and Kump, L. R.: Spatial Patterns of Climate Change across the Paleocene–Eocene Thermal Maximum, Proceedings of the National Academy of Sciences, 119, e2205326 119, https://doi.org/10.1073/pnas.2205326119, 2022.

Tindall, J. C., Valdes, P. J., and Sime, L. C.: Stable Water Isotopes in HadCM3: Isotopic Signature of El Niño–Southern Oscillation and the Tropical Amount Effect, Journal of Geophysical Research, 114, D04 111, https://doi.org/10.1029/2008JD010825, 2009.

1030 Utida, G., Cruz, F. W., Vuille, M., Ampuero, A., Novello, V. F., Maksic, J., Sampaio, G., Cheng, H., Zhang, H., Dias de Andrade, F. R., and Edwards, R. L.: Spatiotemporal ITCZ Dynamics during the Last Three Millennia in Northeastern Brazil and Related Impacts in Modern Human History, Preprint, Proxy Use-Development-Validation/Terrestrial Archives/Holocene, https://doi.org/10.5194/cp-2023-2, 2023.

Valler, V., Brugnara, Y., Franke, J., and Brönnimann, S.: Assimilating Monthly Precipitation Data in a Paleoclimate Data Assimilation Framework, Climate of the Past, 16, 1309–1323, https://doi.org/10.5194/cp-16-1309-2020, 2020.

1035 Valler, V., Franke, J., Brugnara, Y., Samakinwa, E., Hand, R., Lundstad, E., Burgdorf, A.-M., Lipfert, L., Friedman, A. R., and Brönnimann, S.: ModE-RA: a global monthly paleo-reanalysis of the modern era 1421 to 2008, Scientific Data, 11, https://doi.org/10.1038/s41597-023-02733-8, 2024.

Van Rossum, G. and De Boer, J.: Interactively testing remote servers using the Python programming language, CWI quarterly, 4, 283–303, 1991.

1040 Vetra-Carvalho, S., van Leeuwen, P. J., Nerger, L., Barth, A., Altaf, M. U., Brasseur, P., Kirchgessner, P., and Beckers, J.-M.: State-of-the-Art Stochastic Data Assimilation Methods for High-Dimensional Non-Gaussian Problems, Tellus A: Dynamic Meteorology and Oceanography, 70, 1–43, https://doi.org/10.1080/16000870.2018.1445364, 2018.

Vicente-Serrano, S. M., Beguería, S., and López-Moreno, J. I.: A Multiscalar Drought Index Sensitive to Global Warming: The Standardized Precipitation Evapotranspiration Index, Journal of Climate, 23, 1696–1718, https://doi.org/10.1175/2009JCLI2909.1, 2010.

1045 Virtanen, P., Gommers, R., Oliphant, T. E., Haberland, M., Reddy, T., Cournapeau, D., Burovski, E., Peterson, P., Weckesser, W., Bright, J., van der Walt, S. J., Brett, M., Wilson, J., Millman, K. J., Mayorov, N., Nelson, A. R. J., Jones, E., Kern, R., Larson, E., Carey, C. J., Polat, İ., Feng, Y., Moore, E. W., VanderPlas, J., Laxalde, D., Perktold, J., Cimrman, R., Henriksen, I., Quintero, E. A., Harris, C. R., Archibald, A. M., Ribeiro, A. H., Pedregosa, F., van Mulbregt, P., and SciPy 1.0 Contributors: SciPy 1.0: Fundamental Algorithms for Scientific Computing in Python, Nature Methods, 17, 261–272, https://doi.org/10.1038/s41592-019-0686-2, 2020.

1050 Vuille, M., Bradley, R. S., Werner, M., Healy, R., and Keimig, F.: Modeling d18O in precipitation over the tropical Americas: 1. Interannual variability and climatic controls, Journal of Geophysical Research: Atmospheres, 108, https://doi.org/10.1029/2001jd002038, 2003.

Vuille, M., Burns, S. J., Taylor, B. L., Cruz, F. W., Bird, B. W., Abbott, M. B., Kanner, L. C., Cheng, H., and Novello, V. F.: A Review of the South American Monsoon History as Recorded in Stable Isotopic Proxies over the Past Two Millennia, Climate of the Past, 8, 1309–1321, https://doi.org/10.5194/cp-8-1309-2012, 2012.

1055 Wang, J., Emile-Geay, J., Guillot, D., Smerdon, J. E., and Rajaratnam, B.: Evaluating Climate Field Reconstruction Techniques Using Improved Emulations of Real-World Conditions, Climate of the Past, 10, 1–19, https://doi.org/10.5194/cp-10-1-2014, 2014.

Ward, B. M., Wong, C. I., Novello, V. F., McGee, D., Santos, R. V., Silva, L. C., Cruz, F. W., Wang, X., Edwards, R. L., and Cheng, H.: Reconstruction of Holocene coupling between the South American Monsoon System and local moisture variability from speleothem $\delta18O$ and 87Sr/86Sr records, Quaternary Science Reviews, 210, 51–63, https://doi.org/10.1016/j.quascirev.2019.02.019, 2019.

1060 Werner, M., Haese, B., Xu, X., Zhang, X., Butzin, M., and Lohmann, G.: Glacial–Interglacial Changes in $H_2^{18}O$, HDO and Deuterium Excess – Results from the Fully Coupled ECHAM5/MPI-OM Earth System Model, Geoscientific Model Development, 9, 647–670, https://doi.org/10.5194/gmd-9-647-2016, 2016.

Wes McKinney: Data Structures for Statistical Computing in Python, in: Proceedings of the 9th Python in Science Conference, edited by Stéfan van der Walt and Jarrod Millman, pp. 56 – 61, https://doi.org/10.25080/Majora-92bf1922-00a, 2010.

1065 Wong, M. L., Wang, X., Latrubesse, E. M., He, S., and Bayer, M.: Variations in the South Atlantic Convergence Zone over the mid-to-late Holocene inferred from speleothem D18O in central Brazil, Quaternary Science Reviews, 270, 107 178, https://doi.org/10.1016/j.quascirev.2021.107178, 2021.

Yoshimura, K., Kanamitsu, M., Noone, D., and Oki, T.: Historical Isotope Simulation Using Reanalysis Atmospheric Data, Journal of Geophysical Research: Atmospheres, 113, https://doi.org/10.1029/2008JD010074, 2008.

1070 Zhou, J. and Lau, K.: Does a monsoon climate exist over South America?, Journal of climate, 11, 1020–1040, 1998.